RESEARCH ARTICLE

A multi-state model of the CaMKII dodecamer suggests a role for calmodulin in maintenance of autophosphorylation

Matthew C. Pharris[1], **Neal M. Patel**[1], **Tyler G. VanDyk**[1], **Thomas M. Bartol**[2], **Terrence J. Sejnowski**[2,3,4], **Mary B. Kennedy**[5], **Melanie I. Stefan**[2,6,7,8]*, **Tamara L. Kinzer-Ursem**[1]*

1 Weldon School of Biomedical Engineering, Purdue University, West Lafayette, Indiana, United States of America, **2** Salk Institute for Biological Studies, La Jolla, California, United States of America, **3** Institute for Neural Computation, University of California San Diego, La Jolla, California, United States of America, **4** Division of Biological Sciences, University of California San Diego, La Jolla, California, United States of America, **5** Division of Biology and Biological Engineering, California Institute of Technology, Pasadena, California, United States of America, **6** EMBL-European Bioinformatics Institute, Hinxton, United Kingdom, **7** Centre for Discovery Brain Sciences, The University of Edinburgh, Edinburgh, United Kingdom, **8** ZJU-UoE Institute, Zhejiang University, Haining, China

* melanie.stefan@ed.ac.uk (MIS); tursem@purdue.edu (TLKU)

Abstract

Ca^{2+}/calmodulin-dependent protein kinase II (CaMKII) accounts for up to 2 percent of all brain protein and is essential to memory function. CaMKII activity is known to regulate dynamic shifts in the size and signaling strength of neuronal connections, a process known as synaptic plasticity. Increasingly, computational models are used to explore synaptic plasticity and the mechanisms regulating CaMKII activity. Conventional modeling approaches may exclude biophysical detail due to the impractical number of state combinations that arise when explicitly monitoring the conformational changes, ligand binding, and phosphorylation events that occur on each of the CaMKII holoenzyme's subunits. To manage the combinatorial explosion without necessitating bias or loss in biological accuracy, we use a specialized syntax in the software MCell to create a rule-based model of a twelve-subunit CaMKII holoenzyme. Here we validate the rule-based model against previous experimental measures of CaMKII activity and investigate molecular mechanisms of CaMKII regulation. Specifically, we explore how Ca^{2+}/CaM-binding may both stabilize CaMKII subunit activation and regulate maintenance of CaMKII autophosphorylation. Noting that Ca^{2+}/CaM and protein phosphatases bind CaMKII at nearby or overlapping sites, we compare model scenarios in which Ca^{2+}/CaM and protein phosphatase do or do not structurally exclude each other's binding to CaMKII. Our results suggest a functional mechanism for the so-called "CaM trapping" phenomenon, wherein Ca^{2+}/CaM may structurally exclude phosphatase binding and thereby prolong CaMKII autophosphorylation. We conclude that structural protection of autophosphorylated CaMKII by Ca^{2+}/CaM may be an important mechanism for regulation of synaptic plasticity.

Author summary

In the hippocampus, dynamic fluctuation of the size and strength of neuronal connections is thought to underlie learning and memory processes. These fluctuations, called synaptic plasticity, are in-part regulated by the protein calcium/calmodulin-dependent kinase II (CaMKII). During synaptic plasticity, CaMKII becomes activated in the presence of calcium ions (Ca^{2+}) and calmodulin (CaM), allowing it to interact enzymatically with downstream binding partners. Interestingly, activated CaMKII can phosphorylate itself, resulting in state changes that allow CaMKII to be functionally active independent of Ca^{2+}/CaM. Phosphorylation of CaMKII at Thr-286/287 has been shown to be a critical component of learning and memory. To explore the molecular mechanisms that regulate the activity of CaMKII holoenzymes, we use a rule-based approach that reduces computational complexity normally associated with representing the wide variety of functional states that a CaMKII holoenzyme can adopt. Using this approach we observe regulatory mechanisms that might be obscured by reductive approaches. Our results suggest that CaMKII phosphorylation at Thr-286/287 may be stabilized by a mechanism in which CaM structurally excludes phosphatase binding at that site.

Introduction

CaMKII is a protein of interest because of its crucial role in synaptic plasticity [1–5]. In the hippocampus, synaptic plasticity in the post-synapse occurs within mushroom-shaped protrusions called dendritic spines [6]. Synaptic plasticity is dependent on calcium ion (Ca^{2+}) flux through N-methyl-D-aspartate receptors (NMDARs) located on the dendritic spines of the post-synaptic neuron [7]. Depending on the magnitude, frequency, and location of Ca^{2+} flux, synaptic plasticity may produce increases or decreases (or neither) in synaptic strength [8, 9]. Large, higher-frequency Ca^{2+} spikes can induce an enduring up-regulation of synaptic strength, called long-term potentiation (LTP); while weak, lower-frequency Ca^{2+} spikes can induce an enduring down-regulation of synaptic strength, called long-term depression (LTD) [9, 10]. Whether Ca^{2+} spikes induce LTP or LTD depends on relative activation of intracellular protein signaling networks. When Ca^{2+} first enters the dendritic spine, it interacts with a variety of buffer and sensor proteins, chiefly calmodulin (CaM), which has many protein targets in the spine, including CaMKII [5, 11, 12].

The CaMKII holoenzyme contains at least twelve subunits [13–16] arranged as two rings of six. As shown in Fig 1, each CaMKII subunit features an N-terminal kinase domain and C-terminal hub domain [17]. Between the kinase and hub domains is a flexible regulatory domain which lends to the subunit a wide range of movement away from the holoenzyme's central hub. A crystal structure of human alpha-CaMKII expressed in *E. coli* published by Chao *et al.* (2011) shows CaMKII subunits as able to rapidly and stochastically pivot between a "docked" and "undocked" conformation, seemingly mediated by residues on the kinase domain's activation loop and a spur structure on the hub domain (see Fig 3C in [17]), such that a docked subunit may be inaccessible to CaM binding. In contrast, a more recent work using electron microscopy with rat alpha-CaMKII expressed in Sf9 cells suggests that less than 3 percent of subunits exhibit a compact (or docked) conformation [18]. Given the uncertainty in the field, we include subunit docking and undocking in our model, allowing for future exploration of this possible subunit functionality. In addition to docking and undocking, each subunit can be in an "inactive" conformation when the regulatory domain is bound to the kinase domain (Fig 1B), or an "active" conformation when this binding is disrupted by thermodynamic effects. In
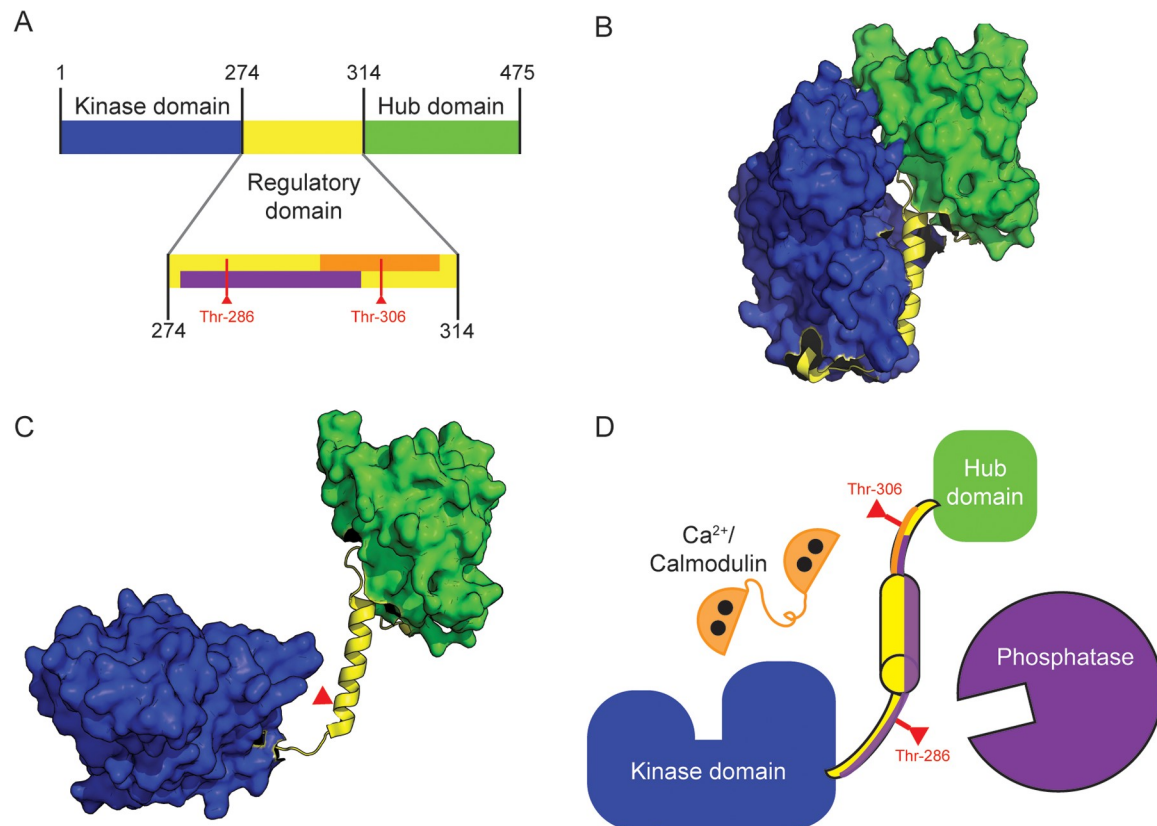
Fig 1. Schematic of CaMKII Subunit Structure. (A) Map of amino acid residues in a CaMKII subunit. The N-terminal kinase domain (blue) approximately spans residues 1–274. The regulatory domain (residues 275–314, yellow) binds to the kinase domain autoinhibiting the kinase activity of the each CaMKII subunit. The putative phosphatase binding site is also shown purple. The Ca^{2+}/CaM binding site is shown in orange. Subunits self-associate via the hub domain (residues 315–475, green) to form multimeric complexes of 12–14 subunit holoenzymes. (B) The "inactive" CaMKII subunit (derived from a crystal structure found on the Protein Data Bank, or PDB, entry code 3SOA) in which the regulatory domain (yellow) is closely associated with the kinase domain (blue). (C) A schematic of the "active" CaMKII subunit. The regulatory domain (yellow) swings away from the kinase domain (blue). This schematic was generated by manually modifying PDB entry 3SOA to illustrate how the regulatory domain may be available for Ca^{2+}/CaM binding and the kinase domain open for substrate binding. (D) Cartoon depiction of all protein species in our model, in which Ca^{2+}/CaM (orange) or phosphatase (purple) may bind to the regulatory domain (yellow) of a CaMKII subunit.

this work, we describe CaMKII subunit activation as highly transient until stabilized by a fully-bound Ca^{2+}/CaM or phosphorylation at Thr-286 [17, 19]. In the active conformation the catalytic domain of a subunit is able to bind and phosphorylate enzymatic substrates. A subunit may spontaneously return to an inactive conformation in the absence of Ca^{2+}/CaM or phosphorylation at Thr-286 [19].

CaMKII can become enzymatically active in the absence of Ca^{2+}/CaM-binding via phosphorylation at Thr-286, which is required for LTP [3, 20]. Importantly, this phenomenon is an autophosphorylation: it is thought to occur when an active subunit phosphorylates neighboring subunits within the same holoenzyme [21, 22]. Autophosphorylation at Thr-286 ("pThr-286") is thought to provide structural stability to a subunit's active conformation (reviewed in [23]) [24]. Because CaMKII plays a key role in the induction of LTP, and ultimately learning and memory (reviewed in [4, 8]), we seek to better understand the biochemical regulation of CaMKII activation and autophosphorylation via computational modeling.

To characterize the spatiotemporal regulation of CaMKII, experimental studies are increasingly complemented by computational models [15, 17, 25–28]. Computational models of

Ca^{2+}-dependent signaling implicate competition, binding kinetics, feedback loops, and spatial effects in regulating enzyme activation [7, 12, 24, 29, 30]. However, fully characterizing these and other mechanisms of CaMKII regulation is impeded by the challenge of accurately portraying the CaMKII holoenzyme. As described by previous work, combinatorial explosion can occur when modeling CaMKII (and similar biomolecules) activation because the protein exhibits a large number of functionally significant and not necessarily inter-dependent states [24, 26, 31–33]. The large number of possible states of CaMKII can neither be explicitly specified nor efficiently evaluated with conventional mass action-based methods. Indeed, for just one CaMKII hexamer ring, we estimate a state space of ~32 billion states, and for the full dodecamer approximately 10^{20} possible states (See Text A in S1 Appendix). The numbers of possible CaMKII states far exceeds the number of CaMKII molecules in a dendritic spine, suggesting that some states rarely occur and thus likely contribute little to protein function. Previous models leverage this observation to reduce the model state space and provide valuable insight to CaMKII binding and autophosphorylation dynamics [24, 33–36]. However, for CaMKII it remains unclear which states functionally participate in synaptic plasticity. Reduced models can inadvertently obscure key mechanisms regulating CaMKII activation and autophosphorylation. To elucidate complex regulatory mechanisms, it may be necessary for models to provide for all possible states *ab initio*.

In this work, we use rule-based model specification and particle-based rule evaluation methods to overcome combinatorial explosion [26, 32, 37]. Rules are conditions, based primarily on experimental observations, that prescribe when an implicitly-defined reaction may occur. At a given iteration, only states that matter for the execution of a particular rule are explicitly declared. States that do not matter to a particular rule can be omitted, a principle that has been paraphrased as "don't care, don't write" [38]. We use rule- and particle-based methods within the spatial-stochastic software MCell 3.3 [30, 39] to present a comprehensive multi-state model of the CaMKII dodecamer. Other simulation platforms can also overcome combinatorial explosion through rule-based model specification (e.g. BioNetGen [40]) or network-free approaches (e.g. NFsim [41]). Unlike other platforms, MCell 3.3 provides both spatial-stochastic and rule-based modeling, although multi-state molecules in MCell 3.3 cannot diffuse. We use MCell 3.3 in anticipation of future MCell versions accounting for multi-state molecule diffusion, and to eventually build on simulations with physiological dendritic spine geometries such as those by Bartol *et al.* (2015) [42].

Here, we validate this rule-based MCell model of CaMKII regulation against current descriptions of the Ca^{2+} frequency-dependence of CaMKII activation. By varying the rules and model parameter values we can simulate different experimental manipulations of CaMKII interaction with Ca^{2+}/CaM and phosphatase and thereby explore various mechanisms regulating CaMKII activity. In particular, we show that Ca^{2+}/CaM is important not only for regulating activation of CaMKII but may also contribute to the maintenance of CaMKII phosphorylation at Thr-286. We hypothesize that by limiting access of phosphatases to CaMKII Thr-286 (perhaps by steric hindrance), Ca^{2+}/CaM may prolong the lifetime of the autophosphorylated state.

Results

Model development

Molecular species. The model contains three protein species: CaM, protein phosphatase, and CaMKII. Ca^{2+}/CaM facilitates CaMKII activation, which leads to autophosphorylation at Thr-286, and phosphatase activity facilitates de-phosphorylation at Thr-286. Both protein phosphatase 1 (PP1) and protein phosphatase 2A (PP2A) have been shown to dephosphorylate

Thr-286, though in different subcellular fractions (reviewed by [21, 43–45]). Here we refer to them generally as protein phosphatase (PP).

CaM and PP are modeled in MCell as conventional cytosolic molecules. Initially, CaM is modeled as having one of two states: un-bound apo-CaM which does not bind CaMKII, and fully-saturated Ca^{2+}/CaM (four Ca^{2+} bound to CaM) which does bind CaMKII similar to previous studies [29, 46]. Notably, we and others have described the importance of sub-saturated Ca^{2+}/CaM states with fewer than 4 Ca^{2+} [12, 24, 33, 47–49]. Thus, we also explore the dynamics of Ca^{2+}-CaM binding and the binding of sub-saturated Ca^{2+}/CaM to CaMKII. However, accounting for sub-saturated Ca^{2+}/CaM would here require a multi-state representation, and because multi-state molecules cannot diffuse in MCell 3.3, we simplify our Ca^{2+}/CaM model to allow CaM to diffuse and interact with a (non-diffusing) multi-state representation of CaMKII. PP is modeled as single-state protein that is constitutively active and able to bind auto-phosphorylated CaMKII subunits. Our representation of constitutively active PP is consistent with previous models such as that by Lisman and Zhabotinsky (2001) [50].

CaMKII is modeled as a multi-subunit, multi-state complex, defined using a specialized model syntax for complex molecules (COMPLEX_MOLECULE) in MCell 3.3 [51]. This syntax allows for explicit representation of individual CaMKII dodecamers with distinguishable subunits. As shown in Fig 2, the holoenzyme is arranged as two directly-apposed, radially-symmetric rings each with six subunits. Each subunit can independently undergo state changes (e.g. subunit docking/undocking, CaM binding, phosphorylation at Thr-298, phosphorylation at Thr-306, binding to PP, see Fig 2). Each of these subunit state changes are represented as five "flags", each standing for a particular state that each CaMKII subunit can adopt. Note that all states are not mutually exclusive (i.e. a subunit can be phosphorylated at Thr-286 and bound to CaM simultaneously). Flags are used in rule evaluation, which occurs at each time step and for each individual subunit. That is, MCell repeatedly evaluates model rules against a given subunit's flags (and those of the neighboring subunits) to determine which state transitions a subunit undertakes at each time step. In the following sub-sections, we describe all CaMKII model flags, the state transitions that apply to each flag, the conditions and rate parameters for each state transition, and related model assumptions. In Fig 2, we visually convey how CaMKII subunits transition between states according to the model's rules. We summarize the state transition rules and rate parameter values in Table A in S1 Appendix.

Flag 1: Subunit docking. Docking is a binary flag that describes CaMKII kinase subunits as either "docked" or "undocked" to the CaMKII central hub. Subunits are instantiated in a docked state but may undergo numerous transitions between docked and undocked over the course of a simulation. At each time step, we assess a rule governing the subunit's transition from a docked to undocked state (see Table A in S1 Appendix). If this rule is satisfied, meaning that the subunit's docking flag is verified as "docked", then the transition to "undocked" is considered. Similarly, we assess a separate rule governing a transition from an undocked to docked state, which requires that the subunit not be bound to CaM and not phosphorylated at Thr-306 [17].

Subunit docking follows the structural model of Chao *et al.*, who showed that a subunit cannot bind CaM as long as the subunit is in a compact conformation, docked to its central hub [17]. Docking implies a two-step process in which the subunit must first un-dock before subsequent CaM-binding, which accounts for the reported difference in binding rate for CaM to CaMKII-derived peptide (1×10^8 $M^{-1}s^{-1}$ [52]) and for CaM to full-length CaMKII-T286A (1.8×10^6 $M^{-1}s^{-1}$ [53]). Taking the ratio of these two rates gives an equilibrium constant for docking of 0.018, which is consistent with estimates by Chao *et al.*, who assumed $K_{docking}$ to fall between 0.01 and 100 [17]. With this equilibrium constant, we estimate kinetic rates for
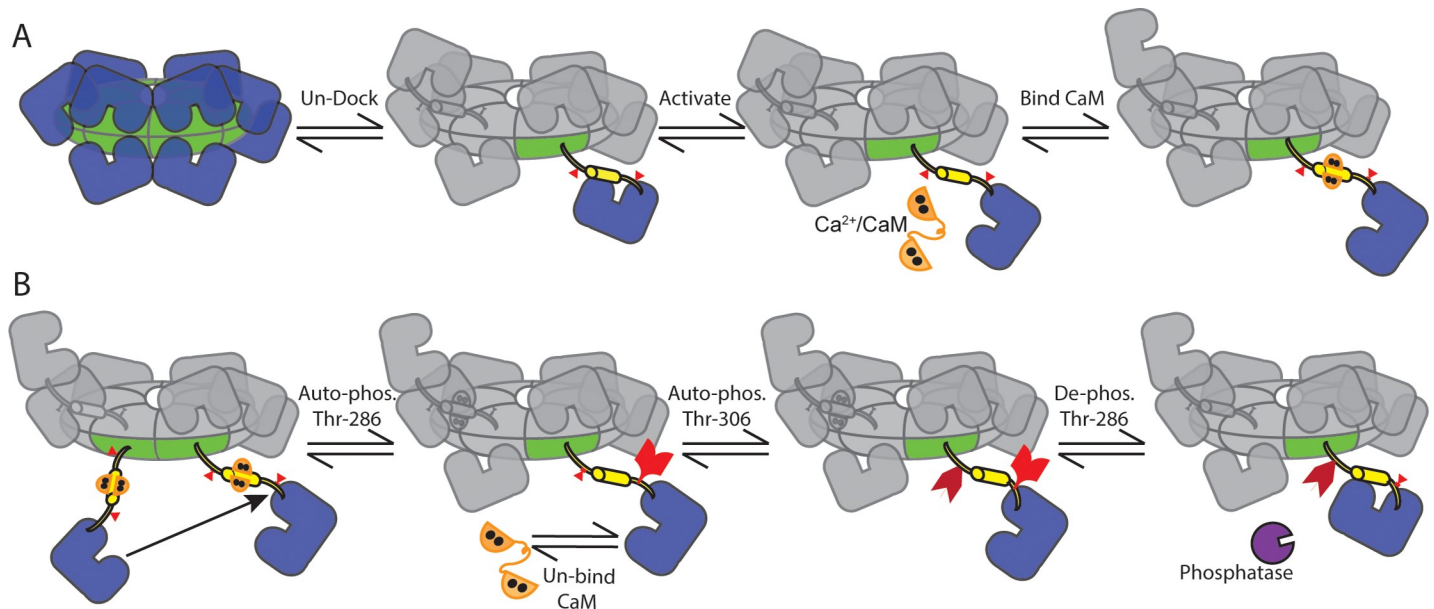
Fig 2. CaMKII holoenzyme state transitions. (A) Our model of CaMKII has twelve individual subunits arranged in two radially symmetric, directly apposed rings. Subunits may spontaneously undock/extend from the central hub or dock/retract (if inactive). Whether docked or undocked, subunits may spontaneously open/activate. (B) If two neighboring subunits are active, one may auto-phosphorylate the other at Thr-286. If auto-phosphorylated (pThr-286), a subunit may remain active even upon un-binding of CaM. A pThr-286 subunit un-bound to CaM may additionally phosphorylate at Thr-306, blocking subsequent re-binding of Ca^{2+}/CaM. A pThr-286 subunit may also bind and become de-phosphorylated by PP (purple).

https://doi.org/10.1371/journal.pcbi.1006941.g002

docking and undocking. For this estimation, we first note that subunit docking involves a structural conformation change on a relatively large scale. Referring to a separate, and notably smaller-scale, conformational change in our model, in which CaM quickly transitions from an initially- to fully-bound state (see Flag 3: CaM Binding), we assume the docked-to-undocked transition to proceed at an order of magnitude slower. We therefore arrive at an assumed rate for k_{dock} of 35 s^{-1}. In turn, this gives an undocking rate $k_{undock} = k_{dock} \times K_{docking}$ of 0.63 s^{-1}, which lies within the range of 0.01 s^{-1} and 100 s^{-1} for k_{undock} assumed by Chao *et al*.

Flag 2: Subunit activation. The activation flag describes CaMKII subunits as either "active" or "inactive". An inactive subunit has no catalytic activity because the regulatory domain is bound to the subunit's catalytic site. Conversely, an active subunit has catalytic activity because the regulatory domain's inhibition of the kinase domain is disrupted. When a subunit is active, Ca^{2+}/CaM and/or other proteins may access and bind CaMKII. In our model, the transition reaction from inactive to active involves no explicit rules (but rather occurs unconditionally and as governed by rates described below). In contrast, two rules inform the conditions for subunit inactivation: that the subunit is 1) not fully-bound to CaM, and 2) not phosphorylated at Thr-286.

To assign rate parameters for this flag, we first note that subunits can fluctuate between inactive and active states rapidly in the absence of Ca^{2+}/CaM (on the order of hundreds of nanoseconds) [19, 54]. Noting this, we set the rate parameter for subunit inactivation at 1×10^7 s^{-1}. Further, Stefan *et al*. determined that the activation probability (in the absence of CaM and phosphorylation) is 0.002, leading us to set our activation rate parameter to 2×10^4 s^{-1} [31]. Thus, we arrive at a model in which CaMKII subunit activation is unstable until stabilized by CaM-binding or autophosphorylation.

Flag 3: CaM binding. CaM binding is a ternary flag meaning that each CaMKII subunit displays one of three states, where CaM may be "unbound", "initially-bound", or "fully

bound". We emphasize that until we present a so-called "9-state-1-step" model of CaM-CaM-KII (see the end of Results), in this paper "CaM" generally refers to fully-saturated Ca^{2+}/CaM (or CaM_4) bound to CaMKII. Our model adapts previous work by Stefan *et al.* (2012) to describe CaM-binding to CaMKII as a two-step process [31]. First, CaM binds to the regulatory domain of a CaMKII subunit (residues 298–312), resulting in a low-affinity "initially bound" CaMKII state, which is compatible with both the inactive (closed) and active (open) subunit conformation. Second, if the initially bound CaMKII opens it may transition to a "fully bound" state that describes the complete, higher-affinity interaction between CaM and CaMKII along residues 291–312 (see Fig 5 in [31]). The transition from an unbound to initially bound state requires the subunit must be: 1) undocked, 2) not PP-bound, and 3) un-phosphorylated at Thr-306. The transition reaction from initially bound to a fully bound state requires just that the subunit already be active/open. Dissociation of CaM from a fully bound CaM--CaMKII state proceeds through the initially bound state before becoming completely unbound from CaMKII.

In order to determine the parameters governing initial binding of CaM to CaMKII, we use data on CaM binding to CaMKII-derived peptides, rather than full-length CaMKII. This is done to separate the intrinsic binding constants from the parameters governing subunit activation/inactivation and docking/undocking. We use the microscopic k_{on} for CaM binding to CaMKII measured by [52], using a CaMKII peptide and fluorescently labeled DA-CaM, as 1×10^8 $M^{-1}s^{-1}$. For the K_D governing initial CaM binding, we use the K_D reported by Tse *et al.* for CaM binding to a low-affinity peptide (CaMKII residues 300–312), which is 5.9×10^{-6} M [55]. From these two parameters, we can compute the dissociation rate of initially-bound CaM from CaMKII: $k_{off\_CaM\_ini} = K_{d\_CaM\_ini} \times k_{on\_CaM} = 590$ s^{-1}. While this rate may seem fast, we emphasize that in our model CaM dissociation happens in two steps, with the transition from fully-bound to initially-bound CaM which we discuss next.

In order to determine the parameters governing the transition from initially-bound to fully-bound CaM to CaMKII, we note that this transition involves a structural compaction of the CaM molecule, which has been measured using fluorescent labels [52, 53]. Using fluorescent labels to analyze the structural compaction of CaM is convenient in its exclusion of effects due to conformational changes within CaMKII subunits or the CaMKII holoenzyme. Thus, we use these measurements as a proxy for CaM binding to a CaMKII peptide and to estimate parameters governing the transition between initially- and fully-bound CaM-CaMKII. Taken from experimental measurements by Torok *et al.*, we identify a transition rate from initially-bound to fully-bound CaM-CaMKII (compaction of CaM) of 350 s^{-1} and from fully-bound back to initially-bound CaM-CaMKII (de-compaction of CaM) of 4×10^{-3} s^{-1} [52]. This means that, in the absence of obstructions to binding, the likelihood of a bound CaM molecule being in the initial binding state (rather than the fully bound state) is 4×10^{-3} / 350 = ~1.1×10^{-5}. This is consistent with a probability of CaM being bound to the high-affinity site of 0.99999 which was derived by Stefan *et al.* (2012) [31].

Flag 4: Phosphorylation at Thr-286. Phosphorylation at the residue Thr-286 is a ternary flag that describes this site as either "un-phosphorylated (uThr-286)", "phosphorylated (pThr-286)", or "phosphatase-bound". We specify four rules to govern the reaction that transitions a subunit from uThr-286 to pThr-286: the subunit 1) be uThr-286, 2) be undocked, 3) be active, and 4) have an active and undocked neighbor subunit in the same holoenzyme ring. Notably, we do not require that a subunit be CaM-bound for autophosphorylation to occur; however, because an un-bound CaMKII subunit's activation is highly transient, we find that CaM-binding is effectively required for autophosphorylation at Thr-286 (shown in Model Validation). Similarly, because pThr-306 (discussed in Flag 5) prohibits CaM-binding, we find that autophosphorylation at Thr-286 effectively requires uThr-306, though we do not explicitly state this

rule. The neighboring subunit's activation flag is considered because autophosphorylation is facilitated by its catalytic site. Our model only considers the counter-clockwise neighbor subunit because, in the absence of experimental observations to the contrary, we assume that steric effects cause autophosphorylation to occur in only one direction about a CaMKII ring, similar to previous work [56, 57]. The rate of autophosphorylation, 1 s^{-1}, at Thr-286 is taken from an earlier study of CaMKII autophosphorylation in the presence of CaM [47].

De-phosphorylation of pThr-286 is facilitated by binding and enzymatic activity of protein phosphatases PP1 and PP2A, here referred to generally as PP [43, 44]. Two rules govern PP binding to a CaMKII subunit (the transition from pThr-286 to a phosphatase-bound state): that the subunit be 1) phosphorylated at Thr-286 (pThr-286) and 2) not be bound to CaM. It has been shown that a majority of autophosphorylated CaMKII in the PSD is dephosphorylated by PP1 [58, 59]; while in brain extracts autophosphorylated CaMKII is mostly dephosphorylated by PP2A [43]. The requirement that CaM be unbound from CaMKII in order for PP to bind to CaMKII is motivated by the observation that simultaneous binding of CaM and PP to the CaMKII regulatory domain may be mutually exclusive due to steric hindrance. CaM, having molecular weight 18 kDa, binds to the CaMKII regulatory domain around residues 290–309 [56, 60, 61], which is at least 4 residues, and at most 23 residues away from Thr-286 (again, see also Fig 5 in [31]). To the best of our knowledge, the peptide binding footprint of neither PP (PP1 nor PP2A) onto CaMKII is fully described. However, both PP1 and PP2A are widely known to target pThr-286 [58, 59, 62] and de-phosphorylate threonine residues nearby alpha helices in other substrates [63, 64]. Additionally, the catalytic subunit of PP1 has a molecular weight of 37 kDa, which is nearly twice that of CaM and more than half that of a CaMKII subunit. Taken together, we hypothesize that the PP binding footprint likely overlaps with the CaM binding site, such that the presence of bound PP likely structurally excludes or impedes upon a subsequent binding of CaM to CaMKII. Similarly, the presence of bound Ca^{2+}/CaM structurally would exclude coincident binding of PP. Starting with Text C in S1 Appendix, we further discuss the quantitative basis of this structural exclusion hypothesis in light of the crystal structure of the PP1-spinophilin interaction (PDB: 3EGG) [65]. In short, PP1 tends to bind substrates at a site >20Å from the PP1 active site. Thus, if the PP1 binding footprint does not actually contain T286, then the furthest likely CaMKII residue of PP1 binding (at least on the hub domain side of T286) is G301, well within the CaM binding footprint (Fig J in S1 Appendix). We examine the regulatory implications of this hypothesis by relaxing the rules of PP binding and requiring only that the subunit be pThr-286. The kinetic rates of PP binding CaMKII are based on values used by Zhabotinsky (2000), using the same catalytic rate of 2 s^{-1} and choosing values for the association (3×10^6 M^{-1}s^{-1}) and dissociation (0.5 s^{-1}) rate constants such that the resulting Michaelis constant (8.3×10^{-7} M) falls in the range used by Zhabotinsky [46].

Flag 5: Phosphorylation at Thr-306. Phosphorylation at the residue Thr-306 is a binary flag that describes this site as either un-phosphorylated ("uThr-306") or phosphorylated ("pThr-306"). We model the transition from uThr-306 to pThr-306 using three rules: that that the subunit be 1) uThr-306, 2) active, and 3) un-bound by CaM. Our model uses a forward rate parameter 50-fold slower than that of phosphorylation at Thr-286, based on past experimental measurements [35, 66]. Over the course of our simulation times, we observe very few pThr-306 transitions and therefore exclude the reverse transition reaction describing de-phosphorylation of pThr-306 into uThr-306. Notably, we do not require that a subunit be pThr-286 as a condition for becoming pThr-306. However, because a subunit's activation is highly transient when un-bound by CaM in our model, the probability of pThr-306 acquisition is quite small if the subunit is not already pThr-286.
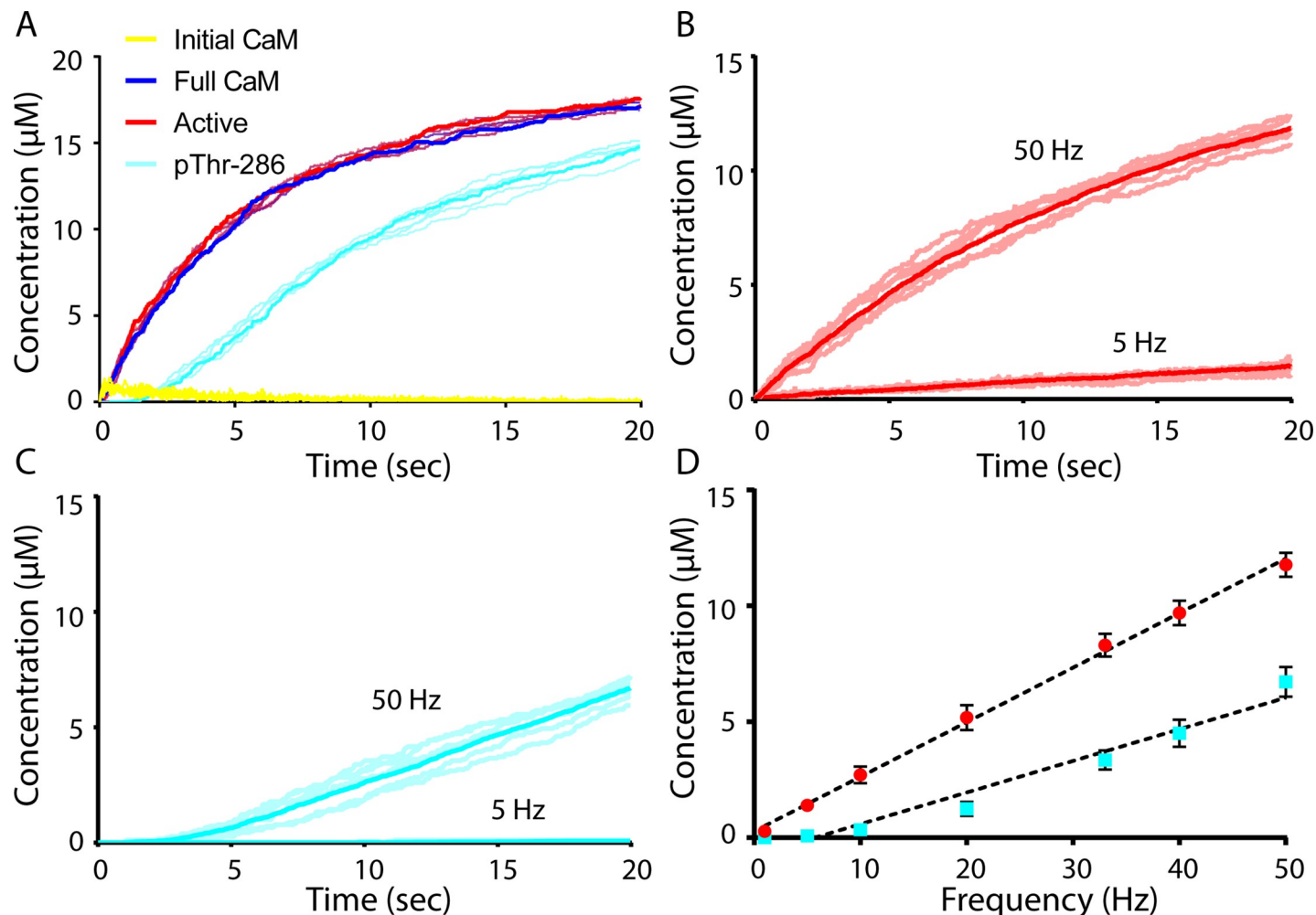
Model validation

Stimulation frequency correlates with subunit activity. To validate our model, we assessed a variety of model outputs under various regimes of Ca^{2+}/CaM stimulation. As a first assessment, we simulated a persistent Ca^{2+}/CaM bolus (note that here we only use the fully saturated CaM_4 as the active form of Ca^{2+}/CaM), similar to experiments by Bradshaw *et al.* (2002), who monitored CaMKII autophosphorylation over time [57]. In Fig 3 we simultaneously monitored the time-course concentration of CaMKII subunit flags indicating: initially-bound Ca^{2+}/CaM, fully-bound Ca^{2+}/CaM, active CaMKII, and pThr-286 (Fig 3). In the persistent, continuous presence of Ca^{2+}/CaM, the concentration of subunits with initially-bound Ca^{2+}/CaM (yellow trace) is noisy and consistently low, implying that initially-bound Ca^{2+}/CaM seems rapidly to either dissociate or proceed to a fully-bound conformation. Fully-bound Ca^{2+}/CaM (red trace) subunit concentrations closely follow those of active CaMKII subunits (dark blue trace) over time, providing evidence that Ca^{2+}/CaM stabilizes CaMKII activation. Indeed, because the difference in concentrations of fully-bound Ca^{2+}/CaM and active CaMKII is always small, we observe that although unbound CaMKII may spontaneously activate, these activated subunits rapidly return to an inactive state and are not likely to progress to a phosphorylated (pThr-286) state. We next observe that the increase of CaMKII autophosphorylation at Thr-286 (cyan trace) over time is strongly associated with increases in the number of subunits that are fully-bound to Ca^{2+}/CaM and active subunits (dark blue and red traces, respectively). This is consistent with previous work showing that Ca^{2+}/CaM must be bound to CaMKII for pThr-286 to occur [56] and CaMKII Ca^{2+}-independent activity is strongly associated CaMKII autophosphorylation at Thr-286 [17, 53, 67, 68]. Furthermore, we observe in Fig 3A that more than 80 percent of CaMKII subunits are autophosphorylated at t = 20sec, which is of similar magnitude and timescale as observed by Bradshaw *et al.* (see Fig 2A in [57]).

Next, we assessed model behavior under low- and high-frequency stimulating conditions. CaMKII activation and autophosphorylation at Thr-286 in response to 5Hz and 50Hz Ca^{2+}/CaM is plotted in Fig 3B and 3C, respectively; 50 seeds were run for each condition, with 6 representative traces (transparent lines) and the average response (bold) plotted. As expected, the data showed significantly greater levels of CaMKII activation and autophosphorylation at 50Hz relative to 5Hz stimulation [12, 20]. Indeed, our results in Fig 3C are comparable to results from Shifman *et al.* (2006), who observed much lower autophosphorylation at low Ca^{2+}/CaM concentrations (less than 2 µM) than at high concentrations (see Fig 4D in [47]).

To further determine how stimulation frequency affects CaMKII activity, the model was stimulated continuously at frequencies ranging from 1Hz to 50 Hz. The concentrations of the various CaMKII states t = 20 seconds of simulation time are plotted as a function of frequency in Fig 3D. We observe a nearly linear correlation between both subunit activation ($R^2 = 0.99$) and pThr-286 ($R^2 = 0.96$). This is consistent with computational results from Chao *et al.*, who developed a stochastic model that also yielded a linear relationship between pThr-286 and stimulation frequency for frequencies greater than 1 Hz [15]. Additionally, our results in Fig 3D show that the model elicits ~5% (~1µM out of 18.24µM total) CaMKII pThr-286 in response to 10Hz stimulation (Fig 3D), which is in general agreement with experimental results given our relatively short pulse width of 10msec (see Fig 4A in [69]). In Fig A in S1 Appendix, we further simulate our model for 20sec at 4Hz Ca^{2+}/CaM using a pulse width of 200msec, yielding ~50% pThr-286, consistent with [69] (see Fig 3B in that paper). Taken together, these results (Fig 3 and Fig A in S1 Appendix) show that our model behaves as expected and is able to produce CaMKII activity and autophosphorylation behaviors similar to previous computational and experimental results.

Fig 3. Validation of the Rule-based Model. Bold traces (A-C) and solid circles (D) are the average of N = 50 executions. For each species (A-C), six representative traces are also shown (semi-transparent lines). (A) Model output resulting from stimulation with a large continuous bolus of Ca^{2+}/CaM. Concentrations of active (red), initially CaM-bound (yellow), fully CaM-bound (blue), and pThr-286 (cyan) subunits. (B) Time-course average concentration (bold trace) of active subunits stimulated by 5 Hz or 50 Hz Ca^{2+}/CaM. (C) Time-course concentration of pThr-286 subunits stimulated continuously by 5 Hz or 50 Hz Ca^{2+}/CaM. (D) Frequency-dependent activation (red) and pThr-286 (cyan) of CaMKII subunits, with SEM error bars. Black dotted traces are linear fits.

https://doi.org/10.1371/journal.pcbi.1006941.g003

Exploring CaMKII holoenzyme phosphorylation

A Thresholded response of CaMKII to Ca^{2+}CaM. CaMKII has long been theorized to exhibit switch-like or bistable behavior, which could underlie the importance of pThr-286 to learning and memory formation [4, 46, 50, 70, 71]. However, experimental efforts have struggled to identify a bistability making CaMKII activity robust to the presence of phosphatases. Recently, Urakubo *et al.* used the chelator EGTA to control single pulses of Ca^{2+} in a mixture of CaM, CaMKII, PP1, and NMDAR peptides, leading to what seemed to be the first direct observation of CaMKII bistability in the presence of NMDAR peptides only [72]. Noting this, we explored whether a spatial stochastic model of the CaMKII dodecamer would exhibit switch-like behavior for concentration parameters of Ca^{2+}, CaM, CaMKII, and PP known to exist in hippocampal spines. We stimulated the model with a set of short Ca^{2+}/CaM input pulses (which could also be reproducible *in vitro*). Importantly, we did not aim to identify true bistability because exploring the many combinations of Ca^{2+}, kinase, and phosphatase
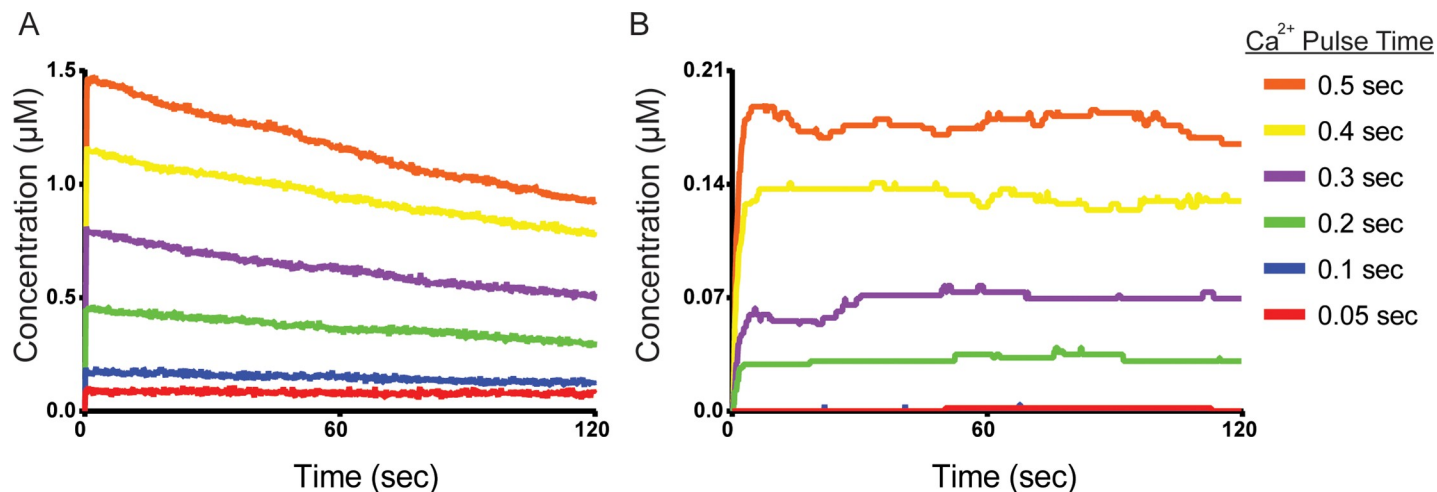
Fig 4. Response to short Ca^{2+}/CaM pulse stimulation. Average concentration of (A) active and (B) pThr-286 CaMKII subunits over time, following Ca^{2+}/CaM stimulating pulses of length 0.05 (red), 0.1 (blue), 0.2 (green), 0.3 (purple), 0.4 (yellow), and 0.5 (orange) seconds. Each trace represents the average of N = 50 executions. See Fig C in S1 Appendix for identical data shown with SEM error bars and over the first two seconds of simulated time. As detailed in Methods, the CaM concentration is here 22.8μM (450 particles).

https://doi.org/10.1371/journal.pcbi.1006941.g004

concentrations was outside the scope of this paper. Instead we wondered if, by stimulating with brief pulses of Ca^{2+}/CaM of variable duration, our model would exhibit switch-reminiscent pThr-286 behavior. Specifically, we hypothesized that there would exist a threshold of time of Ca^{2+}/CaM below which pThr-286 was unachievable and above which pThr-286 was maintained. At stimulation durations above this threshold enough CaMKII autophosphorylation (pThr-286) would occur and self-propagate in balance with de-phosphorylation by PP.

In Fig 4 we exposed our model to single Ca^{2+}/CaM pulses of constant magnitude but of variable duration (similar to Fig 1B in [72]). The model was stimulated with single Ca^{2+}/CaM input pulses of magnitude 22.8 μM and varying duration (0.05, 0.1, 0.2, 0.3, 0.4, or 0.5 sec). Different pulse durations resulted in distinct levels of subunit activation, where longer pulse durations resulted in greater activation and autophosphorylation (p-Thr286) levels, (Fig 4A and 4B, respectively). Interestingly, subunits stimulated by even the shortest pulses of 0.05 or 0.1 sec, appeared to sustain their activation for the simulation period (120 sec). However, these short-pulse (0.05–0.1 sec) stimulations rarely resulted in autophosphorylation (pThr-286, Fig 4B). Longer (0.2–0.5 sec) Ca^{2+}/CaM pulses resulted in greater levels of subunit activation that started declining immediately after the Ca^{2+}/CaM pulse ended (Fig 4A), but elicited pThr-286 levels that were generally sustained for the duration of a simulation (Fig 4B). Taken together, we found that CaMKII may be thresholded at a level of Ca^{2+}/CaM exposure below which pThr-286 is unobserved and above which pThr-286 is achieved and subsequently sustained across several minutes even in the presence of phosphatase.

We also explored how this Ca^{2+}/CaM threshold may depend on the number of directions by which subunits can autophosphorylate their neighbors. Note that in the results up to this point, autophosphorylation was limited to occurring in a single direction, or degree of freedom. That is, subunits could only autophosphorylate their adjacent neighbors in a counterclockwise fashion [17, 56, 57]. We therefore created alternative versions of our model in which autophosphorylation could occur with multiple degrees of freedom: two degrees of freedom in which intra-ring phosphorylation occurs in counter- and clock-wise directions, and three degrees of freedom in which both intra-ring and trans-ring phosphorylation occurs. We used these higher-degree of freedom models to monitor the rates of pThr-286 formation both in

bulk and on an individual subunit basis. As expected, pThr-286 formation and intra-holoenzyme propagation rates increased with increasing degrees of freedom (see Figs E-G in S1 Appendix), though the differences would likely not be distinguishable by bench-top experimentation. In addition, the length of time in which consecutive neighboring subunits remained autophosphorylated also increased with increasing degrees of freedom (Fig G in S1 Appendix). This implied that subunits may be more frequently autophosphorylated on time-average with increasing degrees of freedom. We present this preliminary exploration of the implication of the degrees of freedom, or directionality of CaMKII holoenzyme autophosphorylation, in order to demonstrate various capabilities of the model. We note that current experimental techniques are not sensitive enough to be discriminated between the simulation results. More work needs to be done to better characterize the conditions or possibility of bidirectional autophosphorylation both experimentally and computationally. Future experimental and computational studies could perhaps explore the dependence of autophosphorylation on higher degrees of freedom.

CaM-dependent exclusion of PP1 binding stabilizes autophosphorylation. Fig 4 suggested a threshold of Ca^{2+}/CaM activation beyond which CaMKII remains autophosphorylated, implying a balance between kinase and phosphatase activity. We wondered how a putative balance between CaMKII autophosphorylation and phosphatase activity might be regulated. In the previous experimental work by Urakubo *et al.*, maximally-phosphorylated CaMKII was maintained in the presence of PP1 and NMDAR peptide for as long as 8 hours (at 4˚C). In that work, addition of the kinase inhibitor K252a to phosphorylated CaMKII resulted in a steady decline in pThr-286 towards basal levels, suggesting that maintenance of pThr-286 over time was not due to low phosphatase activity, but rather a recovery of de-phosphorylated subunits back to a phosphorylated state. To recreate inhibition of kinase activity in our model, at time t = 30 sec we introduced a high concentration (18.2 μM) of K252a, enough to bind all CaMKII subunits in the model. K252a binding results in a blocked CaMKII state that cannot be autophosphorylated (see Flag 2 in Table A in S1 Appendix). Importantly, the blocked CaMKII subunit can still be de-phosphorylated at pThr-286. In separate simulations we explored the effects of a phosphatase inhibitor, which was also introduced at t = 30sec. To simulate the introduction of a phosphatase inhibitor, we defined the catalytic rate of de-phosphorylation by PP1 (k_{cat}^{PP1}) as a time-dependent variable that assumed a value of zero at t = 30sec. This implementation of kinase and phosphatase inhibition preserved normal CaM and PP1 binding dynamics.

In these simulations the model was stimulated with 22.8μM CaM_4 (Ca^{2+}/CaM) for 2sec and either no inhibition (control), kinase activity inhibition, or phosphatase inhibition was implemented at 30sec as described above (Fig 5). As expected, inhibiting phosphatase activity (green trace) caused kinase activity to dominate, resulting in a steady increase in pThr-286 compared to the control (black trace). Surprisingly, the kinase-inhibition (blue trace) showed little difference in pThr-286 concentration over time compared to the control. Instead of causing a greater reduction in pThr-286 over time due to phosphatase activity as was expected, inhibition of kinase activity resulted in almost no difference in pThr-286 levels even in the presence of phosphatase activity. We hypothesized that some other, non-enzymatic mechanism in our model was contributing to the maintenance of pThr-286.

In every simulation presented thus far, we assumed that CaM binding to the CaMKII regulatory domain sterically hinders PP binding to the regulatory domain, and vice-versa. This was implemented in the model via a rule that requires a subunit be unbound by CaM in order for PP to bind. To test the role of these exclusions, we created a second version of our model in which PP binding would be allowed regardless of the presence of bound CaM_4, and CaM_4 binding would be allowed regardless of the presence of PP. In contrast to our original
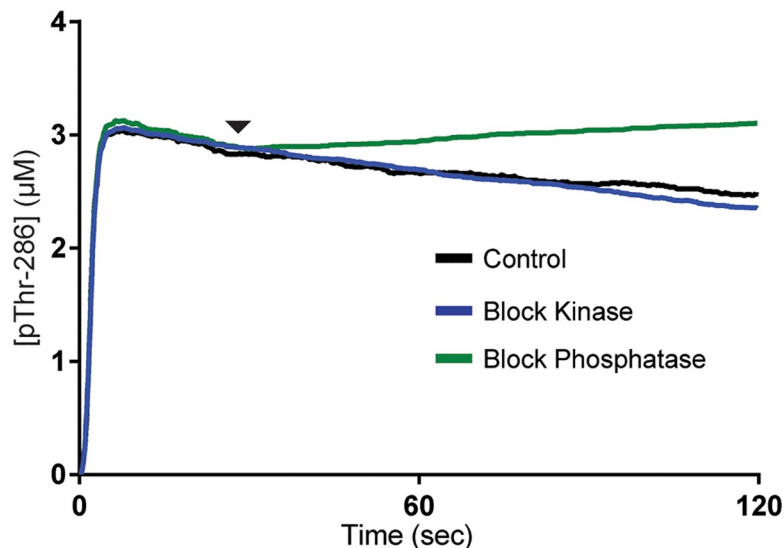
Fig 5. Blocking kinase or phosphatase activity. Average concentration of pThr-286 CaMKII subunits over time. For all traces, the model is stimulated by a 2 sec pulse of Ca^{2+}/CaM. At time t = 30 sec (arrowhead), either a kinase inhibitor (blue trace) or phosphatase inhibitor (green trace) is introduced. No inhibitor is introduced in the control (black trace). Each trace represents the average of N = 50 executions.

https://doi.org/10.1371/journal.pcbi.1006941.g005

"exclusive" model, the "non-exclusive" model required only that a subunit be pThr-286 in order for PP binding to be allowable. In other words, the non-exclusive model allowed Ca^{2+}/CaM and PP to bind CaMKII agnostically of each other. Aside from this rule adjustment, our exclusive and non-exclusive models utilized identical parameters (see Tables A and B in S1 Appendix). As in Fig 5, we selected a Ca^{2+}/CaM bolus time of 2 sec. Again, we monitored both CaMKII activation (Fig 6A and 6B) and pThr-286 (Fig 6C and 6D) over 120 seconds of simulated time. Critically, both the exclusive and non-exclusive models were examined with high (purple trace) and low (orange trace) association rate parameter values for PP binding to CaMKII. Increasing and decreasing the association rate of PP (k_{on}^{PP} is normally set to 3 $\mu M^{-1}sec^{-1}$) to CaMKII by one order of magnitude accounted for parameter uncertainty and provided a magnified view of the signaling effects of CaM-mediated exclusion of PP binding.

Our results suggested that CaM-dependent exclusion of PP is an important regulatory mechanism for maintaining CaMKII autophosphorylation levels. While the PP exclusion rule had little to no effect on the decay of CaMKII subunit de-activation (Fig 6A and Fig 6B, both decay constants -0.0004), pThr-286 (Fig 6C and Fig 6D) was highly influenced by the PP exclusion rule. In the exclusive model (Fig 6C), pThr-286 levels were steady and stable (decay constant -0.0004) despite varying the PP association rate parameter by two orders of magnitude. In contrast, the non-exclusive model (Fig 6D) showed that for a high PP association rate, significant pThr-286 levels remained below 0.5 μM (Fig 6D low k_{on} trace has decay constant -0.006). Moreover, for a low PP association rate, the non-exclusive model attained lower pThr-286 levels compared to the exclusive model, and the pThr-286 levels then declined at a faster rate. We further emphasize the magnitudes of pThr-286 were noticeably influenced by the PP exclusion rule. Upon removing PP exclusion, peak magnitudes of pThr-286 were reduced from 3.2μM (Fig 6C) to ~2.3μM (Fig 6D). It seemed that in order to significantly activate and then maintain pThr-286 over longer time periods, CaMKII required a mechanism regulating phosphatase access, and a regulator of phosphatase access could be CaM itself.
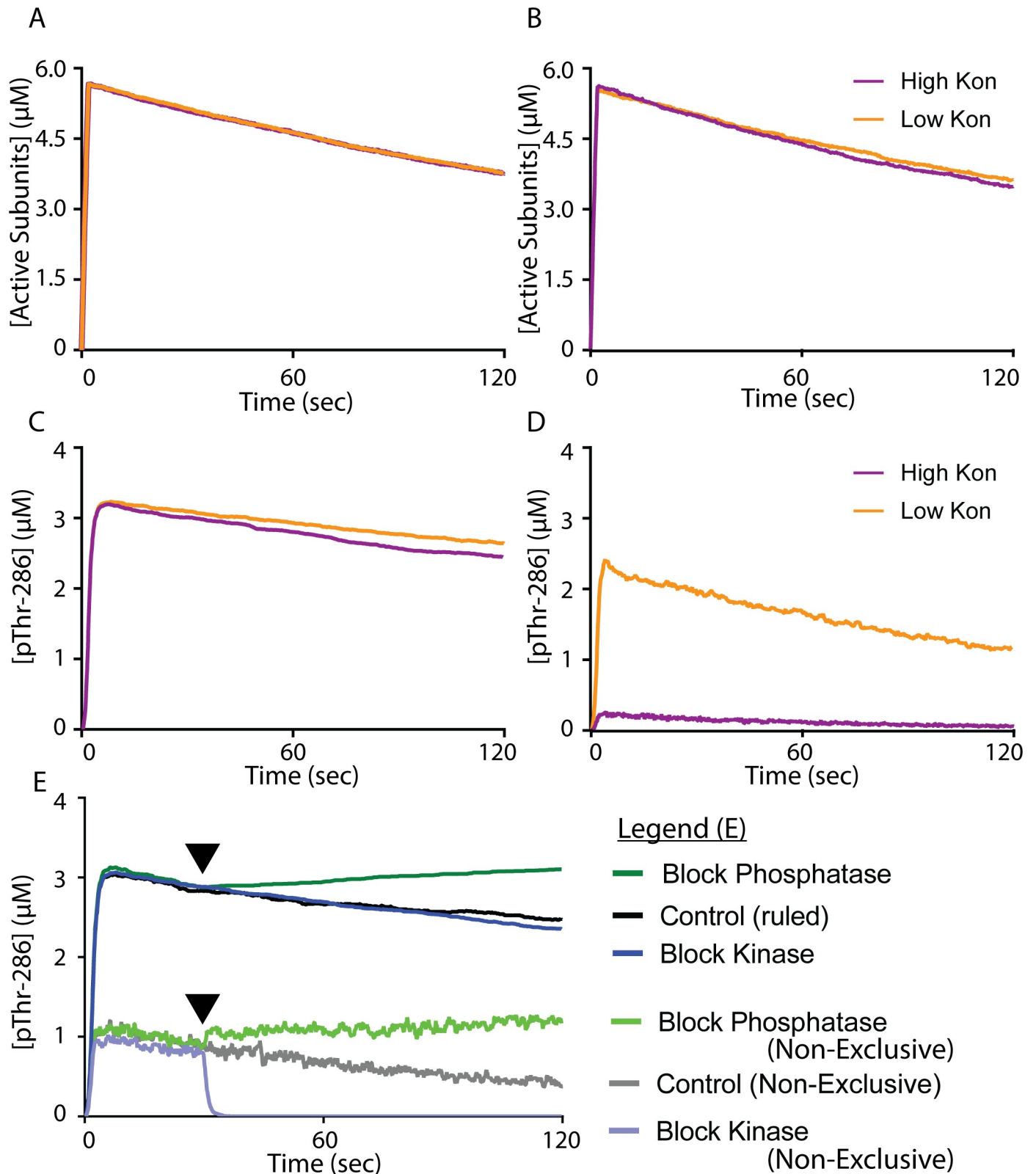
Fig 6. Comparison of Exclusive and Non-exclusive Models. For all traces, models are stimulated by a 2sec pulse of Ca^{2+}/CaM. (A) Active CaMKII subunits over time in our exclusive model. (B) Active CaMKII subunits over time in our non-exclusive model. (C) pThr-286 subunits over time in our exclusive model. (D) pThr-286 subunits over time in our non-exclusive model. (A-D) The parameter value for the rate of PP association (k_{on}^{PP1}) with CaMKII is either increased (purple

traces) or decreased (orange traces) by one order of magnitude. (E) Extension of Fig 5 to include non-exclusive model results; the exclusive model results are also shown in Fig 5. At time t = 30sec (arrows), either a kinase inhibitor (light blue trace) or phosphatase inhibitor (light green trace) is introduced. No inhibitor is introduced in the control (grey trace). All traces are the average of N = 50 executions.

To reinforce our assertion that CaM-dependent structural exclusion of PP binding stabilizes pThr-286, we repeated simulations shown in Fig 5, but with our non-exclusive model. In Fig 6E, we stimulated our non-exclusive model with a 2sec pulse of Ca^{2+}/CaM and then monitored pThr-286 over time. For these simulations, k_{on}^{PP1} was restored to its standard value of $3\ \mu M^{-1}sec^{-1}$. As in Fig 5, in separate simulations we inhibited at t = 30sec either phosphatase activity, kinase activity, or neither (control). The control (grey trace) was reminiscent of results in Fig 6D, in which pThr-286 was achieved but then slowly declined on a steady yet noisy basis. Notably, all non-exclusive model variants were much noisier than their exclusive model counterparts in Fig 6E. Inhibiting phosphatase activity (light green trace) in the non-exclusive model again caused kinase activity to dominate and pThr-286 levels to generally increase over time, similarly to the exclusive model. In contrast to the exclusive model, inhibiting kinase activity (light blue trace) in the non-exclusive model rapidly and totally abolished pThr-286. It seemed that for the non-exclusive model, in which CaM and PP could bind simultaneously, inhibiting kinase activity caused phosphatase activity to dominate. Taken together, these results suggested that in addition to supporting CaMKII subunit activation, CaM also has a role in maintaining CaMKII activity by blocking phosphatase access and thereby slowing down dephosphorylation.

CaM-dependent exclusion of PP1 binding may depend significantly on how we model Ca^{2+}/CaM. Until this point, we have modeled Ca^{2+}/CaM as "2-state-2-step", existing as either Ca^{2+}-unbound apo-CaM or CaM_4 (2 states), which binds CaMKII in an initially- then fully-bound conformation (2 steps). However, previous experimental and computational studies have determined that sub-saturated Ca^{2+}/CaM, with fewer than four Ca^{2+} bound, may significantly bind CaM-binding partners such as CaMKII [24, 47]. Indeed, Pepke et al. [24] and others use a "9-state-1-step" model of Ca^{2+}/CaM, which explicitly accounts for each mode of Ca^{2+}-binding at the CaM N- and C-termini. Importantly, each of the nine Ca^{2+}/CaM states in the Pepke model has unique binding kinetics for CaMKII. We emphasize that these 9-state binding kinetics, which were measured using wild-type CaMKII in vitro, are incompatible with our 2-step CaM-binding model. In other words, a 9-state-2-step CaM-CaMKII model is difficult to parameterize because the available 9-state parameter values inherently account for 2-step CaM-binding. Moreover, the 9-state-2-step model would likely require a multi-state, rule-based model of CaM. And problematically, MCell 3.3 prohibits diffusion for rule-based species. Still, it is important to consider whether sub-saturated Ca^{2+}/CaM states might still be able to structurally exclude, or out-compete, PP1-CaMKII binding.

Although a 9-state-2-step model of CaM-CaMKII binding is currently impractical, a 9-state-1-step model of CaM-CaMKII binding is practical, at least to explore how sub-saturated Ca^{2+}/CaM could exclude PP1-CaMKII binding. For the 9-state-1-step model, we again use MCell 3.3 to describe the multi-state CaMKII holoenzyme, but we modify three of the flags described earlier in this paper. First, we remove the subunit docking and activation flags to reduce model noise and ensure the 9-state CaM-binding parameters remain appropriate. Second, we modify the CaM-binding flag to allow all nine Ca^{2+}/CaM states (including apo-CaM) to bind CaMKII subunits. Thus, whereas in the 2-state-2-step CaMKII model subunit activation is defined by subunit opening, in the 9-state-1-step model activation is defined by CaM-binding. The parameters and reaction network for Ca^{2+}-CaM binding and CaM-CaMKII binding may be found in Pepke et al. (see Fig 2C in [24]), and also refer to Table C in S1

Appendix. With our 9-state-1-step model (MCell code provided in the Purdue University Research Repository with DOI: 10.4231/MV0Z-8Z57, and parameters provided in S1 Appendix), we simulate using identical conditions to those used for Fig 6A–6D, namely with 2000 Ca^{2+} (a CaM-saturating quantity, fully chelated at t = 2sec), 450 CaM particles, and 30 CaMKII holoenzymes. Our 9-state-1-step model results are shown in Fig 7, where we again show that CaMKII subunit activation and pThr-286 levels are maintained on significantly longer time-scales when CaM and PP cannot bind CaMKII simultaneously (Fig 7A and 7D). Compared to Fig 6, activation and pThr-286 levels are both higher and output noise is reduced, likely due to the absence of the activation flag and the fact that in a 9-state model, sub-saturated Ca^{2+}/CaM significantly bind CaMKII and could contribute to its autophosphorylation. These may also explain the lack of difference in the peak magnitudes of pThr-286 in Fig 7C and 7F (compare to the peak magnitudes of Fig 6B and 6D). Specifically, for the 9-state-1-step model in Fig 7 maximal phosphorylation is achievable within 2 sec of Ca^{2+} stimulation, whereas 2 sec is not sufficient for maximal phosphorylation in the 2-state-2-step simulations (Fig 6). Finally, we observe that when only fully-saturated CaM_4 but no other Ca^{2+}/CaM state is allowed to exclude PP (Fig 7B and 7E), model output is virtually identical to the fully non-exclusive case (Fig 7C and 7F). This suggests that sub-saturated Ca^{2+}/CaM states may significantly contribute to PP1 exclusion. Indeed, this may be unsurprising given the affinity of states such as CaM_{2C} for CaMKII (7.4µM), which is only one order of magnitude larger than that of PP1 for CaMKII (0.166µM). Critically, though, in our 9-state-1-step model the CaM_{2C}-CaMKII affinity increases by 1000-fold when a CaMKII is subunit is pThr-286, because we explicitly account for CaM-trapping [73]. Therefore, sub-saturated Ca^{2+}/CaM states are very likely to out-compete PP1 and prevent its binding to CaMKII, at least from a kinetics perspective.

Discussion

In this work, we use rule- and particle-based methods with the software MCell to model the complete CaMKII holoenzyme. Rule-based modeling allows us to account for and monitor multiple CaMKII states simultaneously without eliciting combinatorial explosion. By explicitly accounting for multiple CaMKII states, we can use this model to explore regulatory mechanisms such as the CaM-dependent maintenance of pThr-286 by structural exclusion of phosphatase binding to CaMKII.

Previous multi-state models of CaMKII exist but are different in focus and in scope from the present model. For example, our model is based on an earlier multi-state model by Stefan *et al.* (2012) [31] implemented in the particle-based stochastic simulator StochSim [74]. StochSim accounts for subunit topology (i.e. the user can specify whether a subunit is adjacent to another, and reactions can be neighbor-sensitive), but StochSim does not explicitly account for spatial information. MCell, as a spatial simulator, offers more possibilities to precisely account for spatial effects and to situate models in spatially realistic representations of cellular compartments. In addition, the model by Stefan *et al.* provides only for interactions between adjacent CaMKII molecules on the same hexamer ring and therefore models CaMKII as a hexamer, not a dodecamer. Similarly, another previous model of CaMKII by Michalski and Loew (2012) uses the softwares BioNetGen and VCell to offer an infinite subunit holoenzyme approximation (ISHA) of the CaMKII hexamer [75–77]. The ISHA asserts that under certain enzymatic assumptions, the output of a multi-state CaMKII model is independent of holoenzyme size when the number of subunits exceeds six. However, Michalski's ISHA model is most suitable for systems containing only one holoenzyme structure-dependent reaction such as the autophosphorylation at Thr-286. Additional reactions to describe actin binding [78] or subunit exchange [14, 15] may invalidate Michalski's ISHA, whereas our model can in the
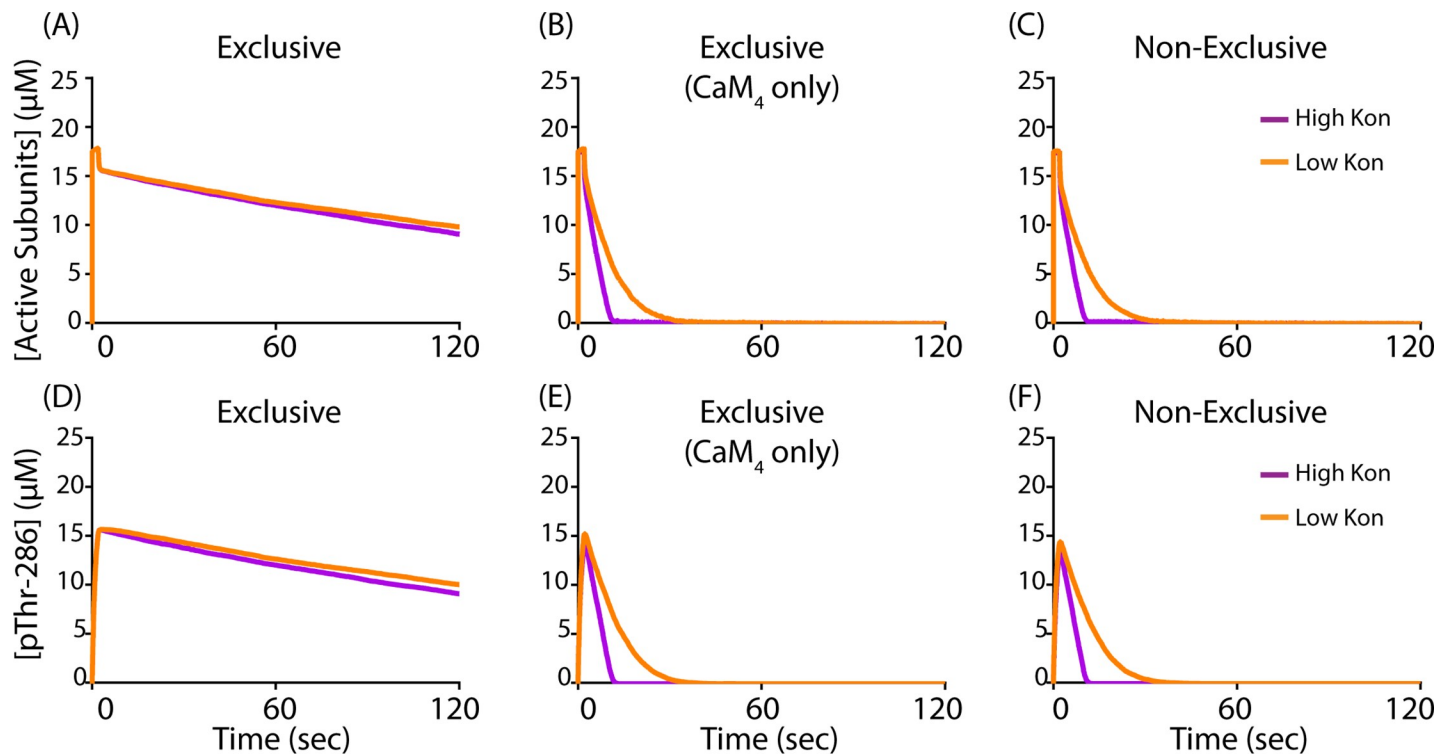
Fig 7. Exclusion in a 9-state-1-step CaM-CaMKII model. For all traces, models are stimulated by a 2sec pulse of Ca^{2+}. (A-C) Active CaMKII subunits over time in our 9-state-1-step model. (D-F) pThr-286 subunits over time. The parameter value for the rate of PP association (k_{on}^{PP1}) with CaMKII is either increased (purple traces) or decreased (orange traces) by one order of magnitude. Because this model version has inherently less output noise, all traces are the average of N = 20 executions.

future readily accommodate additional, holoenzyme structure-dependent phenomena. Finally, a more recent rule-based model of the CaMKII holoenzyme by Li and Holmes [26] offers a detailed representation of how CaM binds to Ca^{2+} and subsequently activates CaMKII subunits, based on earlier results of CaM regulation [79]. Li and Holmes offer valuable and detailed insight into how CaM binding to CaMKII depends on Ca^{2+} dynamics. While our model is less detailed in representing the regulation of CaM itself, our model is much more detailed in representing other aspects of CaMKII regulation, including multiple modes of CaM binding, conformational change, detailed holoenzyme structure, multiple phosphorylation sites, and dephosphorylation. We can in the future expand our MCell model to account for multiple holoenzyme structure-dependent phenomena and simultaneously incorporate this model into the broader Ca^{2+}-dependent signaling network.

This work in-part demonstrates the value of MCell as a rule-based modeling framework. Rule-based modeling accommodates much larger state spaces than is possible using conventional systems of differential equations. Admittedly, not all models (including models of CaMKII) require extensive state spaces, but rule-based modeling results can help justify the assumptions typically used to reduce a state space. For example, our model conditions yield, as shown in Fig 3A, negligible levels of initially-bound CaM compared to other states such as fully-bound CaM or pThr-286. Therefore, it might sometimes be appropriate to exclude an initially-bound CaM state from future implementations in frameworks for which combinatorial explosion is a concern. Aside from addressing combinatorial explosion, rule-based models are especially well-suited to discern otherwise concealed mechanisms, as exemplified by Di Camillo *et al.* who used rule-based models to identify a robustness-lending negative feedback

mechanism in the insulin signaling pathway [49]. Furthermore, MCell describes CaMKII holo-enzymes as discrete particles in space, which will lend realism to future spatial-stochastic models of Ca^{2+}-dependent signaling networks in the dendritic spine, a compartment in which the Law of Mass Action is invalid [24]. This particle-based framework also allows for individual subunit monitoring, which works in conjunction with the Blender software plugin, CellBlender (see Movie A in S1 Appendix).

One of the results of this work is the identification of distinct levels of CaMKII activation and pThr-286 in response to distinct pulses of Ca^{2+}/CaM stimulation. Distinct levels of CaMKII activation could tune the selectivity of CaMKII for certain downstream binding targets such as AMPA receptors or the structural protein PSD-95. If stimulation-dependent tuning of CaMKII activation were observed, it would be reminiscent of other studies that have implicated feedback loops [29] and binding dynamics [24] as regulators of Ca^{2+}-dependent enzyme activation. For example, a recent study suggests that competition is an emergent property that tunes the Ca^{2+} frequency dependence of CaM binding to downstream targets, leading Ca^2+/CaM to set distinct levels of calcineurin- and CaMKII-binding [12]. Similarly, CaMKII itself could preferentially select downstream binding partners as a function of its level of activation by Ca^{2+}/CaM, possibly providing a mechanism by which CaMKII facilitates certain LTP-related molecular events. Additionally, our observation of distinct levels of CaMKII activation and thresholded pThr-286 could be an indication of long-hypothesized switch-like behavior in synaptic plasticity [4, 70]. If switch-like behavior in fact occurs, then pThr-286 is likely maintained by a balance in kinase and phosphatase activity.

While investigating a putative interplay in CaMKII kinase and PP phosphatase activity in maintaining pThr-286 levels, we may have identified a CaM-dependent mechanism that blocks PP binding to CaMKII. In a model that excludes simultaneous binding of CaM and PP to CaMKII, pThr-286 significantly increases upon phosphatase inhibition, yet in the same model kinase inhibition causes little change in pThr-286 over time (Fig 5). In contrast, a non-exclusive model that allows simultaneous binding of CaM and PP shows that introduction of a kinase inhibitor rapidly abolishes pThr-286. These results suggest that CaM-dependent exclusion of PP may provide a stabilizing mechanism. Additionally, we use our MCell-based implementation of the model to monitor transitions between multiple states of distinct subunits within holoenzymes (Fig 8 and Movie A in S1 Appendix).

The major advance of this paper is to present a model of the regulation of 12-subunit CaMKII holoenzyme and its regulation by Ca^{2+}/CaM and protein phosphatase. We assert that CaM-dependent exclusion of PP could provide a functional role for so-called "CaM trapping" [56] and possibly contribute to CaMKII bistability. Indeed, a model by Zhabotinsky (2000) explored CaMKII bistability, indicating that two stable states of pThr-286 would in-part require very high CaMKII concentrations, seemingly to bolster kinase activity in the system [46]. However, the Zhabotinsky model assumes that CaM and PP1 could bind CaMKII simultaneously, possibly exaggerating the ability of PP1 to de-phosphorylate at Thr-286. If PP1 binding were to be encumbered in the Zhabotinsky model, perhaps through CaM-dependent exclusion, then bistability might be achievable at lower CaMKII concentrations.

Previous studies have sought to explore the dependence of CaMKII de-phosphorylation on the presence of Ca^{2+}/CaM. An experiment by Bradshaw *et al.* (2003) quantifies PP1-mediated de-phosphorylation rates of pThr-286 *in vitro*, in the presence or absence of free Ca^{2+} (see Fig 4B in [80]). In both the presence and absence of free Ca^{2+} at 0°C, Bradshaw *et al.* observe that pThr-286 levels decrease over 30 min at similar rates, in conditions with limiting ATP such that CaMKII cannot re-phosphorylate. These results could be interpreted to suggest that PP1 activity is independent of Ca^{2+} and in turn Ca^{2+}/CaM-binding to CaMKII. Note that in the Bradshaw results, regardless of the presence of free Ca^{2+}, CaMKII activation persists for at
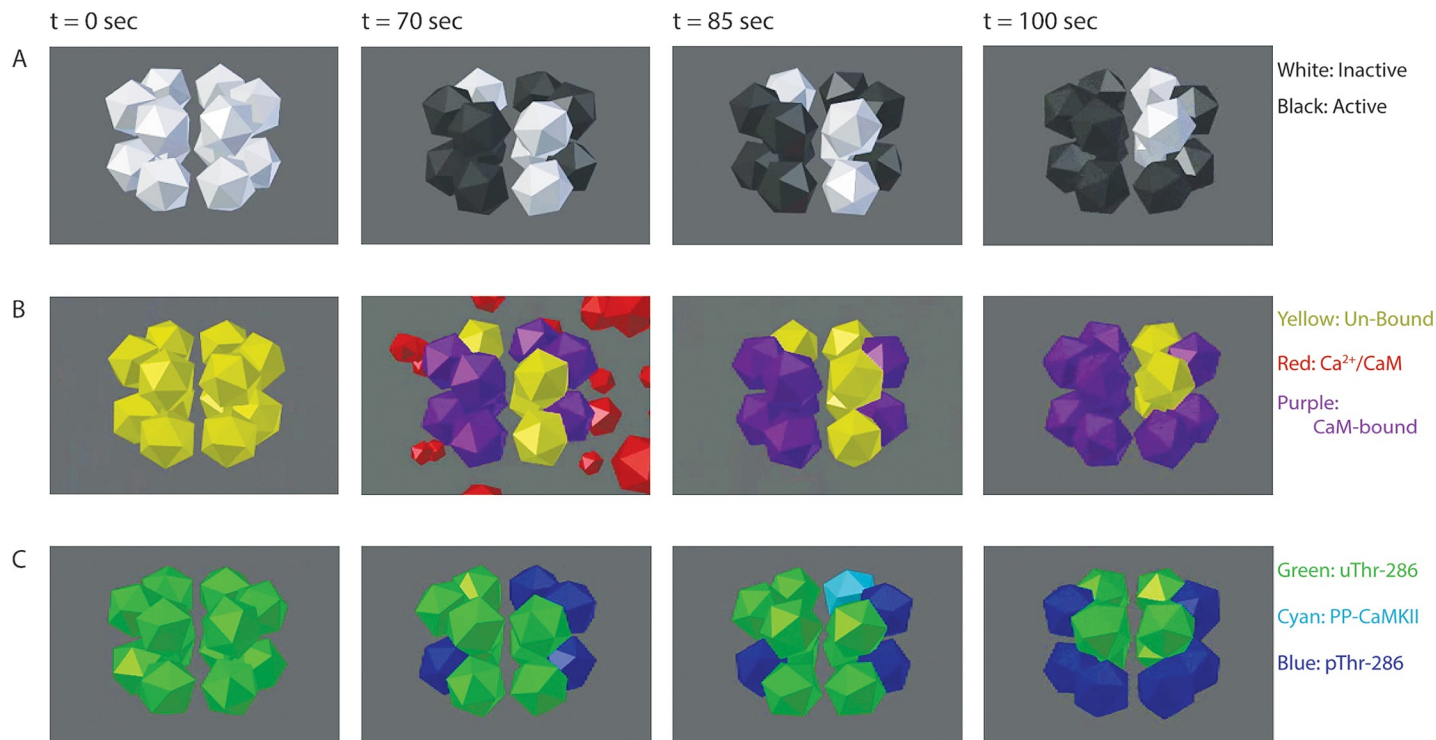
Fig 8. Visualizing individual subunits with MCell and CellBlender. In the exclusive model, PP does not bind a pThr-286 subunit until Ca^{2+}/CaM dissociation (see t = 85 sec, comparing rows B and C). Each frame depicts the same CaMKII holoenzyme, from the same perspective, at identical time points under 50Hz Ca^{2+}/CaM stimulation. Each dodecahedron is a single CaMKII subunit. (A) Inactive CaMKII subunits (white) spontaneously become active (black) and remain active while bound to Ca^{2+}/CaM. (B) Un-bound CaMKII subunits (yellow) will not bind Ca^{2+}/CaM (red) and become Ca^{2+}/CaM-bound (purple) unless the subunit had previously activated. (C) uThr-286 subunits (green) become pThr-286 (blue). If Ca^{2+}/CaM dissociates from a pThr-286 subunit, then PP can bind and form a PP-CaMKII complex (cyan).

https://doi.org/10.1371/journal.pcbi.1006941.g008

least tens of minutes. The persistence of CaMKII activity on relatively long timescales, even in the presence of phosphatase, is consistent with separate experimental results [22, 57, 59, 70, 73]. Our results suggest an alternative interpretation of these and Bradshaw's results. In our model, CaMKII activity persists for many minutes only when CaM excludes PP1. Indeed, the effect of CaM exclusion on the timescale of CaMKII activation is even more pronounced in our 9-state-1-step CaM-binding model results.

Our 9-state-1-step model suggests that following termination of Ca^{2+} flux, sub-saturated Ca^{2+}/CaM states may significantly contribute to PP1-exclusion (Fig K in S1 Appendix). First, this agreement between our 9-state-1-step and primary 2-state-2-step models is a testament to the model's robustness to uncertainty with parameterizing the docking and activation flags. Further, our 9-state-1-step results are also consistent with Bradshaw's results, as seen in Fig 9 of [57] (their supplementary material). Specifically, Bradshaw *et al.* explore in their supplement how CaMKII autophosphorylation levels equilibrate in the presence of various Ca^{2+} concentrations. Importantly, many of the Ca^{2+} concentrations are at levels that would not saturate CaM. Nonetheless, with sub-saturated Ca^{2+}/CaM significant levels of CaMKII autophosphorylation are maintained even by 7.5 hours of incubation, even in the presence of PP1, indicating that sub-saturated Ca^{2+}/CaM states could be playing a key role in maintenance of CaMKII autophosphorylation. In S1 Appendix, we show that the Ca^{2+}/CaM state predominantly responsible for PP1-exclusion following termination of Ca^{2+} stimulation in the 9-state-1-step model is apo-CaM. Apo-CaM remaining bound to CaMKII is consistent with results by

Brown *et al.*, who determine that when free Ca^{2+} levels decrease, Ca^{2+} dissociates from CaM before CaM dissociates from its binding partner [81]. Of course, the affinity of apo-CaM for CaMKII (1.45mM) should be insufficient to out-compete PP1-CaMKII binding (0.16μM). Yet because the 9-state-1-step model explicitly accounts for CaM-trapping by increasing the affinity of pThr-286 subunits for Ca^{2+}/CaM by 1000-fold [73], the affinity of pThr-286 CaMKII for apo-CaM (1.45μM) is within one order of magnitude as that of PP1 (0.16μM). (In the original 2-state-2-step model, we provide for CaM-trapping implicitly through the 2-step CaM-binding.) Thus, apo-CaM may be able to compete with PP1 for CaMKII-binding, but it now remains for future experimental studies to directly quantify the kinetics and/or structure of the apo-CaM interaction with pThr-286 CaMKII. Determining the effect of CaM-trapping on sub-saturated Ca^{2+}/CaM states is outside the scope of the current work. Notably, during dynamic Ca^{2+} flux (S1 Appendix), we observe that non-apo-Ca^{2+}/CaM states such as CaM_{2C} may contribute to maintenance of pThr-286. This indicates that even if structural studies reveal that apo-CaM is insufficient to out-compete PP1, it is possible that CaM-dependent PP1 exclusion could contribute at least somewhat to pThr-286 acquisition and maintenance during Ca^{2+} stimulation. Clearly, further structural and kinetic studies of the CaM-CaMKII and PP1-CaMKII interaction are needed.

CaM-dependent PP exclusion could provide an added layer of robustness to similar mechanisms that may protect pThr-286 from de-phosphorylation. For example, Mullasseril *et al.* (2007) observe that endogenous, PSD-resident PP1 cannot de-phosphorylate CaMKII at pThr-286, whereas adding exogenous PP1 does cause de-phosphorylation [71]. The results by Mullasseril *et al.* suggest that endogenous PP1 is somehow sequestered by the PSD scaffold, and only upon saturation of this scaffold by exogenous PP1 does pThr-286 become de-phosphorylated. Our results indicate that perhaps in addition to saturating the PSD scaffold, the added exogenous PP1 could be out-competing CaM for binding to CaMKII, thereby terminating protection of pThr-286 by CaM. As another example, Urakubo *et al.* suggest that pThr-286 could be protected from PP activity by GluN2B binding, showing that GluN2B peptides are necessary for an apparent CaMKII bistability *in vitro* [72]. Notably, Urakubo *et al.*, when using equal concentrations of CaM and CaMKII subunits, observe a slow and steady decline in pThr-286 upon kinase inhibition that has a similar rate as that seen in the Bradshaw study [80], taking place over the course of hours, which we only observe in our exclusive model. Urakubo *et al.* also mention that when basal levels of Ca^{2+} are set below 0.2 μM, CaMKII autophosphorylation decreases to basal levels within 6 hours, perhaps indicating that GluN2B-dependent exclusion of PP1 is necessary but not sufficient for maintaining pThr-286 levels; sufficiently high levels of Ca^{2+}/CaM may also be required. Overall, it seems scaffold-dependent sequestration of PP1 [71], GluN2B-dependent PP exclusion [72], and CaM-dependent PP exclusion could together provide considerable robustness of pThr-286 to phosphatase activity.

Methods

Simulation methods

In each MCell execution, proteins are instantiated at time zero having random positions within a 0.0328 $μm^3$ (0.0328 fL) cube, with each edge being 0.32μm in length. All proteins are described as three-dimensional volume molecules having the following concentrations: 1.52 μM CaMKII (30 holoenzymes, 18.24 μM and 360 individual CaMKII subunits), 22.8 μM CaM (450 discrete proteins), and 0.86 μM PP1 (17 discrete proteins). Because CaMKII particles are modeled using the specialized COMPLEX_MOLECULE syntax and MCell 3.3 does not accommodate diffusion for such particles, CaMKII is given no diffusion constant. In contrast, CaM and PP1 are simple volume-type molecules that move about the model space with a

diffusion constant 6×10^{-6} cm^2/sec, so chosen to minimize the effects of any possible spatial localizations that may arise during a simulation. We emphasize that because this model does not explore spatial effects and, indeed, does not utilize a physiological spine geometry, using such a relatively fast diffusion parameter ensures that spatial effects do not confound our results. Future models exploring the spatial dependence of CaMKII holoenzyme activity in the dendritic spine may choose to adopt different diffusion parameters. All models are run at a time step of 0.1 μs for a total of either 20 or 120 seconds of simulation time, depending on the model variant.

MCell is a particle-based spatial-stochastic simulation engine. In a particle-based framework, individual protein species are modeled as discrete objects in space, rather than bulk/well-mixed fluids. At each model timestep, MCell calculates each protein particle's subsequent diffusion distance and trajectory, in addition to the particle's probabilities for reacting with any nearby particles. More information about MCell's internal algorithms may be found at mcell.org and in publications such as those by Bartol *et al.* [51]. In short, the particle-based framework in MCell provides for spatial and stochastic considerations because each protein particle has unique spatial coordinates that proceed along random (stochastic) trajectories. Importantly, we assert that spatial-stochastic frameworks may be essential to characterizing CaMKII regulation, because 1) proteins in the spine are spatially organized and 2) protein copy numbers in the spine are low (tens to hundreds each), possibly invalidating the Law of Mass Action. Because MCell models are stochastic and change with each simulation, we average the output of many identical simulations. To ensure that the averaged output converges and is statistically significant, all model variants are repeated 50 times each.

CaM activation/inactivation is modeled by a pair of forcing functions which serve as a proxy for Ca^{2+} flux. Both forcing functions are time-dependent square waves and inform the rates at which free CaM transitions between states (see Fig B in S1 Appendix) Eq 1 rapidly transitions all free CaM towards an active (Ca^{2+}/CaM) state, and Eq 2 rapidly transitions all free CaM towards an inactive (apo-CaM) state.

$$F_{activation}(t) = \begin{cases} 100000000, t = n_i \\ 0, t \neq n_i \end{cases} \tag{1}$$

$$F_{inactivation}(t) = \begin{cases} 0, t = n_i \\ 100000000, t \neq n_i \end{cases} \tag{2}$$

For both Eqs 1 and 2, n = i/f where i is the number of time step iterations and f is frequency. Time t iterates at 0.01sec intervals for the complete duration of a simulation. Eqs 1 and 2 therefore yield a peak width of 0.01sec regardless of frequency, which allows us to directly compare the effect of different Ca^{2+}/CaM frequencies on CaMKII activity, without having to account for variable amounts of Ca^{2+}/CaM exposure per pulse. In separate simulations without frequency dependence (i.e. Ca^{2+}/CaM is continuously available to CaMKII), Eq 1 is adjusted to always fulfill the t = n$_i$ condition. Similarly, for pulse simulations in which Ca^{2+}/CaM becomes withdrawn or blocked, Eqs 1 and 2 are given abbreviated time domains.

All MCell code and associated files are available online at Github, the Purdue University Research Repository, and the University of Edinburgh Repository. Material will be made available upon publication.

Supporting information

S1 Appendix. This document enumerates the model parameters, discusses combinatorial explosion, shows alternative visualizations of select data, and discusses the quantitative basis for PP1/CaM mutual exclusion from CaMKII binding.
(DOCX)

Acknowledgments

The authors thank Nicolas LeNovere, Elizabeth Phillips, Kaisa Ejendal, and David Umulis for their helpful advice and comments on the manuscript.

Author Contributions

Conceptualization: Matthew C. Pharris, Thomas M. Bartol, Terrence J. Sejnowski, Mary B. Kennedy, Melanie I. Stefan, Tamara L. Kinzer-Ursem.

Data curation: Matthew C. Pharris, Melanie I. Stefan, Tamara L. Kinzer-Ursem.

Formal analysis: Matthew C. Pharris, Mary B. Kennedy, Melanie I. Stefan, Tamara L. Kinzer-Ursem.

Funding acquisition: Terrence J. Sejnowski, Mary B. Kennedy, Melanie I. Stefan, Tamara L. Kinzer-Ursem.

Investigation: Matthew C. Pharris, Tyler G. VanDyk, Melanie I. Stefan, Tamara L. Kinzer-Ursem.

Methodology: Matthew C. Pharris, Thomas M. Bartol, Terrence J. Sejnowski, Melanie I. Stefan, Tamara L. Kinzer-Ursem.

Project administration: Terrence J. Sejnowski, Mary B. Kennedy, Melanie I. Stefan, Tamara L. Kinzer-Ursem.

Resources: Thomas M. Bartol, Terrence J. Sejnowski, Melanie I. Stefan, Tamara L. Kinzer-Ursem.

Software: Matthew C. Pharris, Neal M. Patel, Tyler G. VanDyk, Thomas M. Bartol, Terrence J. Sejnowski, Melanie I. Stefan, Tamara L. Kinzer-Ursem.

Supervision: Terrence J. Sejnowski, Mary B. Kennedy, Melanie I. Stefan, Tamara L. Kinzer-Ursem.

Validation: Matthew C. Pharris, Tyler G. VanDyk, Melanie I. Stefan, Tamara L. Kinzer-Ursem.

Visualization: Matthew C. Pharris, Neal M. Patel, Melanie I. Stefan, Tamara L. Kinzer-Ursem.

Writing – original draft: Matthew C. Pharris, Melanie I. Stefan, Tamara L. Kinzer-Ursem.

Writing – review & editing: Matthew C. Pharris, Neal M. Patel, Tyler G. VanDyk, Mary B. Kennedy, Melanie I. Stefan, Tamara L. Kinzer-Ursem.

References

1. Erondu NE, Kennedy MB. Regional distribution of type-II Ca2+ calmodulin-dependent protein-kinase in rat-brain. J Neurosci. 1985; 5(12):3270–7. https://doi.org/10.1523/JNEUROSCI.05-12-03270.1985 PMID: 4078628

2. Kennedy MB. Regulation of synaptic transmission in the central nervous-system—long-term potentiation. Cell. 1989; 59(5):777–87. https://doi.org/10.1016/0092-8674(89)90601-6 PMID: 2556217

3. Silva AJ, Stevens CF, Tonegawa S, Wang YY. Deficient hippocampal long-term potentiation in alpha-calcium-calmodulin kinase-II mutant mice. Science. 1992; 257(5067):201–6. https://doi.org/10.1126/science.1378648 PMID: 1378648

4. Lisman J, Schulman H, Cline H. The molecular basis of CaMKII function in synaptic and behavioural memory. Nat Rev Neurosci. 2002; 3(3):175–90. https://doi.org/10.1038/nrn753 PMID: 11994750

5. Kennedy MB. Synaptic signaling in learning and memory. Cold Spring Harbor Perspect Biol. 2013;8. https://doi.org/10.1101/cshperspect.a016824 PMID: 24379319

6. Harris KM. Structure, development, and plasticity of dendritic spines. Curr Opin Neurobiol. 1999; 9 (3):343–8. https://doi.org/10.1016/s0959-4388(99)80050-6 PMID: 10395574

7. Evans RC, Morera-Herreras T, Cui YH, Du K, Sheehan T, Kotaleski JH, et al. The effects of NMDA subunit composition on calcium influx and spike timing-dependent plasticity in striatal medium spiny neurons. PLoS Comput Biol. 2012; 8(4):13. https://doi.org/10.1371/journal.pcbi.1002493 PMID: 22536151

8. Kennedy MB. Synaptic signaling in learning and memory. Cold Spring Harbor Perspect Biol. 2016; 8 (2):16. https://doi.org/10.1101/cshperspect.a016824 PMID: 24379319

9. Sjostrom PJ, Nelson SB. Spike timing, calcium signals and synaptic plasticity. Curr Opin Neurobiol. 2002; 12(3):305–14. https://doi.org/10.1016/s0959-4388(02)00325-2 PMID: 12049938

10. He Y, Kulasiri D, Samarasinghe S. Systems biology of synaptic plasticity: A review on N-methyl-D-aspartate receptor mediated biochemical pathways and related mathematical models. Biosystems. 2014; 122:7–18. https://doi.org/10.1016/j.biosystems.2014.06.005 PMID: 24929130

11. Xia ZG, Storm DR. The role of calmodulin as a signal integrator for synaptic plasticity. Nat Rev Neurosci. 2005; 6(4):267–76. https://doi.org/10.1038/nrn1647 PMID: 15803158

12. Romano DR, Pharris MC, Patel NM, Kinzer-Ursem TL. Competitive tuning: Competition's role in setting the frequency-dependence of Ca2+-dependent proteins. PLoS Comput Biol. 2017; 13(11):26. https://doi.org/10.1371/journal.pcbi.1005820 PMID: 29107982

13. Bennett MK, Erondu NE, Kennedy MB. Purification and characterization of a calmodulin-dependent protein-kinase that is highly concentrated in brain. J Biol Chem. 1983; 258(20):2735–44.

14. Stratton M, Lee IH, Bhattacharyya M, Christensen SM, Chao LH, Schulman H, et al. Activation-triggered subunit exchange between CaMKII holoenzymes facilitates the spread of kinase activity. eLife. 2014; 3:28. https://doi.org/10.7554/eLife.01610 PMID: 24473075

15. Bhattacharyya M, Stratton MM, Going CC, McSpadden ED, Huang Y, Susa AC, et al. Molecular mechanism of activation-triggered subunit exchange in Ca2+/ calmodulin-dependent protein kinase II. eLife. 2016; 5:32. https://doi.org/10.7554/eLife.13045

16. Rosenberg OS, Deindl S, Sung RJ, Nairn AC, Kuriyan J. Structure of the autoinhibited kinase domain of CaMKII and SAXS analysis of the holoenzyme. Cell. 2005; 123(5):849–60. https://doi.org/10.1016/j.cell.2005.10.029 PMID: 16325579

17. Chao LH, Stratton MM, Lee IH, Rosenberg OS, Levitz J, Mandell DJ, et al. A mechanism for tunable autoinhibition in the structure of a human ca2+/calmodulin-dependent kinase II holoenzyme. Cell. 2011; 146(5):732–45. https://doi.org/10.1016/j.cell.2011.07.038 PMID: 21884935

18. Myers JB, Zaegel V, Coultrap SJ, Miller AP, Bayer KU, Reichow SL. The CaMKII holoenzyme structure in activation-competent conformations. Nat Commun. 2017; 8:14. https://doi.org/10.1038/s41467-017-00024-6

19. Hoffman L, Stein RA, Colbran RJ, McHaourab HS. Conformational changes underlying calcium/calmodulin-dependent protein kinase II activation. Embo J. 2011; 30(7):1251–62. https://doi.org/10.1038/emboj.2011.40 PMID: 21343908

20. Giese KP, Fedorov NB, Filipkowski RK, Silva AJ. Autophosphorylation at Thr(286) of the alpha calcium-calmodulin kinase II in LTP and learning. Science. 1998; 279(5352):870–3. https://doi.org/10.1126/science.279.5352.870 PMID: 9452388

21. Colbran RJ, Fong YL, Schworer CM, Soderling TR. Regulatory interactions of the calmodulin-binding, inhibitory, and autophosphorylation domains of Ca2+/calmodulin-dependent protein kinase-II. Journal of Biological Chemistry. 1988; 263(34):18145–51. PMID: 2848027

22. Miller SG, Kennedy MB. Regulation of brain type-II Ca-2+ calmodulin-dependent protein-kinase by autophosphorylation—a Ca-2+-triggered molecular switch. Cell. 1986; 44(6):861–70. https://doi.org/10.1016/0092-8674(86)90008-5 PMID: 3006921

23. Hudmon A, Schulman H. Neuronal Ca2+/calmodulin-dependent protein kinase II: The role of structure and autoregulation in cellular function. Ann Rev Biochem. 2002; 71:473–510. https://doi.org/10.1146/annurev.biochem.71.110601.135410 PMID: 12045104

24. Pepke S, Kinzer-Ursem T, Mihalas S, Kennedy MB. A dynamic model of interactions of Ca2+, calmodulin, and catalytic subunits of ca2+/calmodulin-dependent protein kinase II. PLoS Comput Biol. 2010; 6 (2):15. https://doi.org/10.1371/journal.pcbi.1000675 PMID: 20168991

25. Li Y, Holmes WR. Comparison of CaMKinase II activation in a dendritic spine computed with deterministic and stochastic models of the NMDA synaptic conductance. Neurocomputing. 2000; 32:1–7. https://doi.org/10.1016/s0925-2312(00)00137-5

26. Li X, Holmes WR. Biophysical attributes that affect CaMKII activation deduced with a novel spatial stochastic simulation approach. PLOS Computational Biology; 2018.

27. Holmes WR. Models of calmodulin trapping and CaM kinase II activation in a dendritic spine. J Comput Neurosci. 2000; 8(1):65–85. https://doi.org/10.1023/a:1008969032563 PMID: 10798500

28. Zeng SY, Holmes WR. The effect of noise on CaMKII activation in a dendritic spine during LTP induction. J Neurophysiol. 2010; 103(4):1798–808. https://doi.org/10.1152/jn.91235.2008 PMID: 20107130

29. Hayer A, Bhalla US. Molecular switches at the synapse emerge from receptor and kinase traffic. PLoS Comput Biol. 2005; 1(2):137–54. https://doi.org/10.1371/journal.pcbi.0010020 PMID: 16110334

30. Keller DX, Franks KM, Bartol TM, Sejnowski TJ. Calmodulin activation by calcium transients in the postsynaptic density of dendritic spines. PLoS One. 2008; 3(4):16. https://doi.org/10.1371/journal.pone.0002045 PMID: 18446197

31. Stefan MI, Marshall DP, Le Novere N. Structural analysis and stochastic modelling suggest a mechanism for calmodulin trapping by CaMKII. PLoS One. 2012; 7(1):14. https://doi.org/10.1371/journal.pone.0029406 PMID: 22279535

32. Stefan MI, Bartol TM, Sejnowski TJ, Kennedy MB. Multi-state modeling of biomolecules. PLoS Comput Biol. 2014; 10(9):9. https://doi.org/10.1371/journal.pcbi.1003844 PMID: 25254957

33. Li L, Stefan MI, Le Novere N. Calcium input frequency, duration and amplitude differentially modulate the relative activation of calcineurin and CaMKII. PLoS One. 2012; 7(9):17. https://doi.org/10.1371/journal.pone.0043810 PMID: 22962589

34. Zhabotinsky AM, Camp RN, Epstein IR, Lisman JE. Role of the neurogranin concentrated in spines in the induction of long-term potentiation. J Neurosci. 2006; 26(28):7337–47. https://doi.org/10.1523/JNEUROSCI.0729-06.2006 PMID: 16837580

35. Lucic V, Greif GJ, Kennedy MB. Detailed state model of CaMKII activation and autophosphorylation. Eur Biophys J Biophys Lett. 2008; 38(1):83–98. https://doi.org/10.1007/s00249-008-0362-4 PMID: 18769913

36. Byrne MJ, Waxham MN, Kubota Y. The impacts of geometry and binding on CaMKII diffusion and retention in dendritic spines. J Comput Neurosci. 2011; 31(1):1–12. https://doi.org/10.1007/s10827-010-0293-9 PMID: 21104309

37. Johnson T, Bartol T, Sejnowski T, Mjolsness E. Model reduction for stochastic CaMKII reaction kinetics in synapses by graph-constrained correlation dynamics. Phys Biol. 2015; 12(4):16. https://doi.org/10.1088/1478-3975/12/4/045005 PMID: 26086598

38. Chylek LA, Harris LA, Tung CS, Faeder JR, Lopez CF, Hlavacek WS. Rule-based modeling: a computational approach for studying biomolecular site dynamics in cell signaling systems. Wiley Interdiscip Rev-Syst Biol. 2014; 6(1):13–36. https://doi.org/10.1002/wsbm.1245 PMID: 24123887

39. Sejnowski TJ, Poggio T. Computational modeling methods for neuroscientists foreword. In: DeSchutter E, editor. Computational Modeling Methods for Neuroscientists. Computational Neuroscience-MIT. Cambridge: Mit Press; 2009. p. VII-+.

40. Blinov ML, Faeder JR, Goldstein B, Hlavacek WS. BioNetGen: software for rule-based modeling of signal transduction based on the interactions of molecular domains. Bioinformatics. 2004; 20(17):3289–91. https://doi.org/10.1093/bioinformatics/bth378 PMID: 15217809

41. Sneddon MW, Faeder JR, Emonet T. Efficient modeling, simulation and coarse-graining of biological complexity with NFsim. Nat Methods. 2011; 8(2):177–U12. https://doi.org/10.1038/nmeth.1546 PMID: 21186362

42. Bartol TM, Keller DX, Kinney JP, Bajaj CL, Harris KM, Sejnowski TJ, et al. Computational reconstitution of spine calcium transients from individual proteins. Frontiers in synaptic neuroscience. 2015; 7:17. https://doi.org/10.3389/fnsyn.2015.00017 PMID: 26500546

43. Strack S, Barban MA, Wadzinski BE, Colbran RJ. Differential inactivation of postsynaptic density-associated and soluble Ca2+/calmodulin-dependent protein kinase II by protein phosphatases 1 and 2A. Journal of Neurochemistry. 1997; 68(5):2119–28. https://doi.org/10.1046/j.1471-4159.1997.68052119.x PMID: 9109540

44. Strack S, Kini S, Ebner FF, Wadzinski BE, Colbran RJ. Differential cellular and subcellular localization of protein phosphatase 1 isoforms in brain. J Comp Neurol. 1999; 413(3):373–84. PMID: 10502246

45. Schworer CM, Colbran RJ, Soderling TR. Reversible generation of a Ca-2+-independent form of Ca-2 +(calmodulin)-dependent protein kinase-II by an autophosphorylation mechanism. J Biol Chem. 1986; 261(19):8581–4. PMID: 3722161

46. Zhabotinsky AM. Bistability in the Ca2+/calmodulin-dependent protein kinase-phosphatase system. Biophys J. 2000; 79(5):2211–21. https://doi.org/10.1016/S0006-3495(00)76469-1 PMID: 11053103

47. Shifman JM, Choi MH, Mihalas S, Mayo SL, Kennedy MB. Ca2+/calmodulin-dependent protein kinase II (CaMKII) is activated by calmodulin with two bound calciums. Proc Natl Acad Sci U S A. 2006; 103 (38):13968–73. https://doi.org/10.1073/pnas.0606433103 PMID: 16966599

48. Blackwell KT. Approaches and tools for modeling signaling pathways and calcium dynamics in neurons. J Neurosci Methods. 2013; 220(2):131–40. https://doi.org/10.1016/j.jneumeth.2013.05.008 PMID: 23743449

49. Forest A, Swulius MT, Tse JKY, Bradshaw JM, Gaertner T, Waxham MN. Role of the N- and C-lobes of calmodulin in the activation of Ca(2+)/calmodulin-dependent protein kinase II. Biochemistry. 2008; 47 (40):10587–99. https://doi.org/10.1021/bi8007033 PMID: 18795794

50. Lisman JE, Zhabotinsky AM. A model of synaptic memory: A CaMKII/PP1 switch that potentiates transmission by organizing an AMPA receptor anchoring assembly. Neuron. 2001; 31(2):191–201. https://doi.org/10.1016/s0896-6273(01)00364-6 PMID: 11502252

51. Bartol T, Derkach M, Faeder J. MCell. Encyclopedia of computational neuroscience; 2015. p. 1673–76.

52. Torok K, Tzortzopoulos A, Grabarek Z, Best SL, Thorogate R. Dual effect of ATP in the activation mechanism of brain Ca2+/calmodulin-dependent protein kinase II by Ca2+/calmodulin. Biochemistry. 2001; 40(49):14878–90. https://doi.org/10.1021/bi010920+ PMID: 11732908

53. Tzortzopoulos A, Torok K. Mechanism of the T286A-mutant alpha CaMKII interactions with Ca2+/calmodulin and ATP. Biochemistry. 2004; 43(21):6404–14. https://doi.org/10.1021/bi036224m PMID: 15157074

54. Hoffman L, Chandrasekar A, Wang X, Putkey JA, Waxham MN. Neurogranin alters the structure and calcium binding properties of calmodulin. J Biol Chem. 2014; 289(21):14644–55. https://doi.org/10.1074/jbc.M114.560656 PMID: 24713697

55. Tse JKY, Giannetti AM, Bradshaw JM. Thermodynamics of calmodulin trapping by Ca2+/calmodulin-dependent protein kinase II: Subpicomolar K-d determined using competition titration calorimetry. Biochemistry. 2007; 46(13):4017–27. https://doi.org/10.1021/bi700013y PMID: 17352496

56. Hanson PI, Meyer T, Stryer L, Schulman H. Dual role of calmodulin in autophosphorylation of multifunctional CaM kinase may underlie decoding of calcium signals. Neuron. 1994; 12(5):943–56. https://doi.org/10.1016/0896-6273(94)90306-9 PMID: 8185953

57. Bradshaw JM, Hudmon A, Schulman H. Chemical quenched flow kinetic studies indicate an intraholoenzyme autophosphorylation mechanism for Ca2+/calmodulin-dependent protein kinase II. J Biol Chem. 2002; 277(23):20991–8. https://doi.org/10.1074/jbc.M202154200 PMID: 11925447

58. Shields SM, Ingebritsen TS, Kelly PT. Identification of protein phosphatase-1 in synaptic junctions— dephosphorylaton of endogenous calmodulin-dependent kinase-II and synapse-enriched phosphoproteins. J Neurosci. 1985; 5(12):3414–22. https://doi.org/10.1523/JNEUROSCI.05-12-03414.1985 PMID: 3001244

59. Dosemeci A, Reese TS. Inhibition of endogenous phosphatase in a postsynaptic density fraction allows extensive phosphorylation of the major postsynaptic density protein. J Neurochem. 1993; 61(2):550–5. https://doi.org/10.1111/j.1471-4159.1993.tb02158.x PMID: 8393087

60. Waxham MN, Tsai AL, Putkey JA. A mechanism for calmodulin (CaM) trapping by CaM-kinase II defined by a family of CaM-binding peptides. Journal of Biological Chemistry. 1998; 273(28):17579–84. https://doi.org/10.1074/jbc.273.28.17579 PMID: 9651352

61. Meador WE, Means AR, Quiocho FA. Target enzyme recognition by calmodulin—2.4-angstrom structure of a calmodulin-peptide complex. Science. 1992; 257(5074):1251–5. https://doi.org/10.1126/science.1519061 PMID: 1519061

62. Mulkey RM, Endo S, Shenolikar S, Malenka RC. Involvement of a calcineurin/inhibitor-1 phosphatase cascade in hippocampal long-term depression. Nature. 1994; 369(6480):486–8. https://doi.org/10.1038/369486a0 PMID: 7515479

63. Ragusa MJ, Dancheck B, Critton DA, Nairn AC, Page R, Peti W. Spinophilin directs protein phosphatase 1 specificity by blocking substrate binding sites. Nat Struct Mol Biol. 2010; 17(4):459–U100. https://doi.org/10.1038/nsmb.1786 PMID: 20305656

64. Kelker MS, Page R, Peti W. Crystal structures of protein phosphatase-1 bound to nodularin-r and tautomycin: a novel scaffold for structure-based drug design of serine/threonine phosphatase inhibitors. J Mol Biol. 2009; 385(1):11–21. https://doi.org/10.1016/j.jmb.2008.10.053 PMID: 18992256

65. Hsieh-Wilson LC, Allen PB, Watanabe T, Nairn AC, Greengard P. Characterization of the neuronal targeting protein spinophilin and its interactions with protein phosphatase-1. Biochemistry. 1999; 38 (14):4365–73. https://doi.org/10.1021/bi982900m PMID: 10194355

66. Payne ME, Fong YL, Ono T, Colbran RJ, Kemp BE, Soderling TR, et al. Calcium calmodulin-dependent protein kinase-ii—characterization of distinct calmodulin binding and inhibitory domains. J Biol Chem. 1988; 263(15):7190–5. PMID: 2835367

67. Miller P, Zhabotinsky AM, Lisman JE, Wang XJ. The stability of a stochastic CaMKII switch: Dependence on the number of enzyme molecules and protein turnover. PLoS Biol. 2005; 3(4):705–17. https://doi.org/10.1371/journal.pbio.0030107 PMID: 15819604

68. Kolodziej SJ, Hudmon A, Waxham MN, Stoops JK. Three-dimensional reconstructions of calcium/calmodulin dependent (CaM) kinase II alpha and truncated CaM kinase II alpha reveal a unique organization for its structural core and functional domains. J Biol Chem. 2000; 275(19):14354–9. https://doi.org/10.1074/jbc.275.19.14354 PMID: 10799516

69. De Koninck P, Schulman H. Sensitivity of CaM kinase II to the frequency of Ca2+ oscillations. Science. 1998; 279(5348):227–30. https://doi.org/10.1126/science.279.5348.227 PMID: 9422695

70. Lisman JE. A mechanism for memory storage insensitive to molecular turnover—a bistable autophosphorylating kinase. Proc Natl Acad Sci U S A. 1985; 82(9):3055–7. https://doi.org/10.1073/pnas.82.9.3055 PMID: 2986148

71. Mullasseril P, Dosemeci A, Lisman JE, Griffith LC. A structural mechanism for maintaining the 'on-state' of the CaMKII memory switch in the post-synaptic density. J Neurochem. 2007; 103(1):357–64. https://doi.org/10.1111/j.1471-4159.2007.04744.x PMID: 17877639

72. Urakubo H, Sato M, Ishii S, Kuroda S. In vitro reconstitution of a CaMKII memory switch by an nmda receptor-derived peptide. Biophys J. 2014; 106(6):1414–20. https://doi.org/10.1016/j.bpj.2014.01.026 PMID: 24655517

73. Meyer T, Hanson PI, Stryer L, Schulman H. Calmodulin trapping by calcium-calmodulin dependent protein-kinase. Science. 1992; 256(5060):1199–202. https://doi.org/10.1126/science.256.5060.1199 PMID: 1317063

74. Le Novere N, Shimizu TS. STOCHSIM: modelling of stochastic biomolecular processes. Bioinformatics. 2001; 17(6):575–6. https://doi.org/10.1093/bioinformatics/17.6.575 PMID: 11395441

75. Michalski PJ, Loew LM. CaMKII activation and dynamics are independent of the holoenzyme structure: an infinite subunit holoenzyme approximation. Phys Biol. 2012; 9(3):13. https://doi.org/10.1088/1478-3975/9/3/036010 PMID: 22683827

76. Slepchenko BM, Schaff JC, Macara I, Loew LM. Quantitative cell biology with the virtual cell. Trends Cell Biol. 2003; 13(11):570–6. https://doi.org/10.1016/j.tcb.2003.09.002 PMID: 14573350

77. Harris LA, Hogg JS, Tapia JJ, Sekar JAP, Gupta S, Korsunsky I, et al. BioNetGen 2.2: advances in rule-based modeling. Bioinformatics. 2016; 32(21):3366–8. https://doi.org/10.1093/bioinformatics/btw469 PMID: 27402907

78. Khan S, Conte I, Carter T, Bayer KU, Molloy JE. Multiple CaMKII binding modes to the actin cytoskeleton revealed by single-molecule imaging. Biophys J. 2016; 111(2):395–408. https://doi.org/10.1016/j.bpj.2016.06.007 PMID: 27463141

79. Linse S, Helmersson A, Forsen S. Calcium-binding to calmodulin and its globular domains. J Biol Chem. 1991; 266(13):8050–4. PMID: 1902469

80. Bradshaw JM, Kubota Y, Meyer T, Schulman H. An ultrasensitive Ca2+/calmodulin-dependent protein kinase II-protein phosphatase 1 switch facilitates specificity in postsynaptic calcium signaling. Proc Natl Acad Sci USA. 2003; 100(18):10512–7. https://doi.org/10.1073/pnas.1932759100 PMID: 12928489

81. Brown SE, Martin SR, Bayley PM. Kinetic control of the dissociation pathway of calmodulin-peptide complexes. J Biol Chem. 1997; 272(6):3389–97. https://doi.org/10.1074/jbc.272.6.3389 PMID: 9013581

Appendix S1

Supplemental Material:

A Multi-State Model of the CaMKII Dodecamer Suggests

a Role for Calmodulin in Maintenance of Autophosphorylation

Matthew C. Pharris, Neal M. Patel, Tyler G. VanDyk, Thomas M. Bartol, Terrence J. Sejnowski, Mary B.

Kennedy, Melanie I. Stefan, and Tamara L. Kinzer-Ursem

Contents:

Table A. CaMKII model state transitions, grouped by flag, with rates and conditions provided.

Flag	State Transition	Rate	Condition (Rule)	References
1) **Docking**	Docked → Undocked	0.63 s^{-1}	Subunit Flag 1 == Docked	[1-3], this paper
	Undocked → Docked	35 s^{-1}	Subunit Flag 3 == Unbound Subunit Flag 5 == uThr-306	[1-3], this paper
2) **Activation**	Inactive → Active	2×10^4 s^{-1}	*None*	[4]
	Active → Inactive	1×10^7 s^{-1}	Subunit Flag 4 == uThr-286 <mark>Subunit Flag 3 != Fully-Bound</mark>	[5, 6], this paper
Select executions:	Active + K252a → Blocked	1×10^9 s^{-1}	*None*	Large value
3) **Ca^{2+}/CaM Binding**	Unbound + CaM$_4$ → Initially-Bound	1×10^8 M^{-1}s^{-1}	Subunit Flag 1 == Undocked Subunit Flag 4 != PP1-bound Subunit Flag 5 == uThr-306	[1, 4]
	Initially-Bound → Fully-Bound	350 s^{-1}	Subunit Flag 2 == Active	[1]
	Fully-Bound → Initially-Bound	4×10^{-3} s^{-1}	*None*	[1]
	Initially-Bound → Unbound + CaM$_4$	590 s^{-1}	*None*	[1, 7], this paper
4) **Phosphorylation (Thr-286)**	uThr-286 → pThr-286	1 s^{-1}	Subunit Flag 1 == Undocked Neighbor Flag 1 == Undocked Subunit Flag 2 == Active Neighbor Flag 2 == Active	[8]
	pThr-286 + PP1 → PP1-bound	3×10^6 M^{-1}s^{-1}	Subunit Flag 3 == Unbound	Derived from [9]
	PP1-bound → uThr-286 + PP1	2 s^{-1}	*None*	[9]
	PP1-bound → pThr-286 + PP1	0.5 s^{-1}	*None*	Derived from [9]
5) **Phosphorylation (Thr-306)**	uThr-306 → pThr-306	0.02 s^{-1}	Subunit Flag 1 == Undocked Subunit Flag 2 == Active Subunit Flag 3 == Unbound	[10, 11], this paper

Note: Double equal signs (==) denote the conditional "true" and the exclamation-equal sign (!=) denotes the conditional "false" statement.

Table B. Transitions, rates parameters, conditions, and citations for the non-exclusive model.

Flag	State Transition	Rate	Condition (Rule)	References
1) **Docking**	Docked → Undocked	0.63 s^{-1}	Subunit Flag 1 == Docked	[1-3], this paper
	Undocked → Docked	35 s^{-1}	Subunit Flag 3 == Unbound Subunit Flag 5 == uThr-306	[1-3], this paper
2) **Activation**	Inactive → Active	$2\times10^4\text{ s}^{-1}$	*None*	[4]
	Active → Inactive	$1\times10^7\text{ s}^{-1}$	Subunit Flag 4 == uThr-286 Subunit Flag 3 != Fully-Bound	[5, 6], this paper
Select executions:	Active + K252a → Blocked	$1\times10^9\text{ s}^{-1}$	*None*	Large value
3) **Ca²⁺/CaM Binding**	Unbound + CaM₄ → Initially-Bound	$1\times10^8\text{ M}^{-1}\text{s}^{-1}$	Subunit Flag 1 == Undocked Subunit Flag 5 == uThr-306	[1, 4]
	Initially-Bound → Fully-Bound	350 s^{-1}	Subunit Flag 2 == Active	[1]
	Fully-Bound → Initially-Bound	$4\times10^{-3}\text{ s}^{-1}$	*None*	[1]
	Initially-Bound → Unbound + CaM₄	590 s^{-1}	*None*	[1, 7], this paper
4) **Phosphorylation (Thr-286)**	uThr-286 → pThr-286	1 s^{-1}	Subunit Flag 1 == Undocked Neighbor Flag 1 == Undocked Subunit Flag 2 == Active Neighbor Flag 2 == Active	[8]
	pThr-286 + PP1 → PP1-bound	$\mathbf{3\times10^6\text{ M}^{-1}\text{s}^{-1}}$	*None*	Derived from [9]
	PP1-bound → uThr-286 + PP1	2 s^{-1}	*None*	[9]
	PP1-bound → pThr-286 + PP1	0.5 s^{-1}	*None*	Derived from [9]
5) **Phosphorylation (Thr-306)**	uThr-306 → pThr-306	0.02 s^{-1}	Subunit Flag 1 == Undocked Subunit Flag 2 == Active Subunit Flag 3 == Unbound	[10, 11], this paper

Note: Differences in Flags 3 & 4 between Table A and Table B.

Table S3. Transitions, rates parameters, and conditions for the exclusive 9-state-1-step model.

Flag	State Transition	Rate	Condition (Rule)	References
1) Ca²⁺/CaM Binding	Unbound + CaM_0 → CaM_0-CaMKII	$0.0038 \mu M^{-1}s^{-1}$	Flag 2 != PP1-bound Flag 3 == uThr-306	[12]
	Unbound + CaM_{1C} → CaM_{1C}-CaMKII	$0.059 \ \mu M^{-1}s^{-1}$	Flag 2 != PP1-bound Flag 3 == uThr-306	[12]
	Unbound + CaM_{2C} → CaM_{2C}-CaMKII	$0.92 \ \mu M^{-1}s^{-1}$	Flag 2 != PP1-bound Flag 3 == uThr-306	[12]
	Unbound + CaM_{1N} → CaM_{1N}-CaMKII	$0.022 \ \mu M^{-1}s^{-1}$	Flag 2 != PP1-bound Flag 3 == uThr-306	[12]
	Unbound + CaM_{2N} → CaM_{2N}-CaMKII	$0.12 \ \mu M^{-1}s^{-1}$	Flag 2 != PP1-bound Flag 3 == uThr-306	[12]
	Unbound + CaM_{1N1C} → CaM_{1N1C}-CaMKII	$0.33 \ \mu M^{-1}s^{-1}$	Flag 2 != PP1-bound Flag 3 == uThr-306	[12]
	Unbound + CaM_{2N1C} → CaM_{2N1C}-CaMKII	$1.9 \ \mu M^{-1}s^{-1}$	Flag 2 != PP1-bound Flag 3 == uThr-306	[12]
	Unbound + CaM_{1N2C} → CaM_{1N2C}-CaMKII	$5.2 \ \mu M^{-1}s^{-1}$	Flag 2 != PP1-bound Flag 3 == uThr-306	[12]
	Unbound + CaM_4 → CaM_4-CaMKII	$30 \ \mu M^{-1}s^{-1}$	Flag 2 != PP1-bound Flag 3 == uThr-306	[12]
	CaM_0-CaMKII → Unbound+CaM_0	$5.5 \ sec^{-1}$	*None*	[12]
	CaM_{1C}-CaMKII → Unbound+CaM_{1C}	$6.1 \ sec^{-1}$	*None*	[12]
	CaM_{2C}-CaMKII → Unbound+CaM_{2C}	$6.8 \ sec^{-1}$	*None*	[12]
	CaM_{1N}-CaMKII → Unbound+CaM_{1N}	$3.1 \ sec^{-1}$	*None*	[12]
	CaM_{2N}-CaMKII → Unbound+CaM_{2N}	$1.7 \ sec^{-1}$	*None*	[12]
	CaM_{1N1C}-CaMKII → Unbound+CaM_{1N1C}	$3.4 \ sec^{-1}$	*None*	[12]
	CaM_{2N1C}-CaMKII → Unbound+CaM_{2N1C}	$1.9 \ sec^{-1}$	*None*	[12]
	CaM_{1N2C}-CaMKII → Unbound+CaM_{1N2C}	$3.8 \ sec^{-1}$	*None*	[12]
	CaM_4-CaMKII → Unbound+CaM_4	$1.7 \ sec^{-1}$	*None*	[12]
	CaM_0-CaMKII → Unbound+CaM_0	$5.5/1000 \ sec^{-1}$	Flag 2 == pThr-286	[13]
	CaM_{1C}-CaMKII → Unbound+CaM_{1C}	$6.1/1000 \ sec^{-1}$	Flag 2 == pThr-286	[13]
	CaM_{2C}-CaMKII → Unbound+CaM_{2C}	$6.8/1000 \ sec^{-1}$	Flag 2 == pThr-286	[13]
	CaM_{1N}-CaMKII → Unbound+CaM_{1N}	$3.1/1000 \ sec^{-1}$	Flag 2 == pThr-286	[13]
	CaM_{2N}-CaMKII → Unbound+CaM_{2N}	$1.7/1000 \ sec^{-1}$	Flag 2 == pThr-286	[13]
	CaM_{1N1C}-CaMKII → Unbound+CaM_{1N1C}	$3.4/1000 \ sec^{-1}$	Flag 2 == pThr-286	[13]
	CaM_{2N1C}-CaMKII → Unbound+CaM_{2N1C}	$1.9/1000 \ sec^{-1}$	Flag 2 == pThr-286	[13]
	CaM_{1N2C}-CaMKII → Unbound+CaM_{1N2C}	$3.8/1000 \ sec^{-1}$	Flag 2 == pThr-286	[13]
	CaM_4-CaMKII → Unbound+CaM_4	$1.7/1000 \ sec^{-1}$	Flag 2 == pThr-286	[13]
	Ca^{2+} + CaM_0-CaMKII ↔ CaM_{1C}-CaMKII	$44 \ \mu M^{-1}s^{-1}$; $33 \ sec^{-1}$	*None*	[12]
	Ca^{2+} + CaM_0-CaMKII ↔ CaM_{1N}-CaMKII	$76 \ \mu M^{-1}s^{-1}$; $300 \ sec^{-1}$	*None*	[12]
	Ca^{2+} + CaM_{1C}-CaMKII ↔ CaM_{2C}-CaMKII	$44 \ \mu M^{-1}s^{-1}$; $2.7 \ sec^{-1}$	*None*	[12]
	Ca^{2+} + CaM_{1C}-CaMKII ↔ CaM_{1N1C}-CaMKII	$76 \ \mu M^{-1}s^{-1}$; $300 \ sec^{-1}$	*None*	[12]
	Ca^{2+} + CaM_{1N}-CaMKII ↔ CaM_{2N}-CaMKII	$76 \ \mu M^{-1}s^{-1}$; $29.6 \ sec^{-1}$	*None*	[12]
	Ca^{2+} + CaM_{1N}-CaMKII ↔ CaM_{1N1C}-CaMKII	$44 \ \mu M^{-1}s^{-1}$; $33 \ sec^{-1}$	*None*	[12]
	Ca^{2+} + CaM_{1N1C}-CaMKII ↔ CaM_{1N2C}-CaMKII	$44 \ \mu M^{-1}s^{-1}$; $2.7 \ sec^{-1}$	*None*	[12]
	Ca^{2+} + CaM_{2N}-CaMKII ↔ CaM_{2N1C}-CaMKII	$44 \ \mu M^{-1}s^{-1}$; $33 \ sec^{-1}$	*None*	[12]
	Ca^{2+} + CaM_{2C}-CaMKII ↔ CaM_{1N2C}-CaMKII	$76 \ \mu M^{-1}s^{-1}$; $300 \ sec^{-1}$	*None*	[12]
	Ca^{2+} + CaM_{2C}-CaMKII ↔ CaM_{1N2C}-CaMKII	$76 \ \mu M^{-1}s^{-1}$; $29.6 \ sec^{-1}$	*None*	[12]
	Ca^{2+} + CaM_{2N1C}-CaMKII ↔ CaM_4-CaMKII	$44 \ \mu M^{-1}s^{-1}$; $2.7 \ sec^{-1}$	*None*	[12]
	Ca^{2+} + CaM_{1N2C}-CaMKII ↔ CaM_4-CaMKII	$76 \ \mu M^{-1}s^{-1}$; $29.6 \ sec^{-1}$	*None*	[12]

2)	Phosphorylation (Thr-286)	uThr-286 → pThr-286	1 s^{-1}	Flag 1 != Unbound	[8]
		pThr-286 + PP1→ PP1-bound	3×10^6 M^{-1}s^{-1}	Flag 1 == Unbound	[9]
		PP1-bound → uThr-286 + PP1	2 s^{-1}	*None*	[9]
		PP1-bound → pThr-286 + PP1	0.5 s^{-1}	*None*	[9]
3)	Phosphorylation (Thr-306)	uThr-306 → pThr-306	0.02 s^{-1}	Flag 1 != Unbound	[10, 11], this paper

Note: Parameters for Ca^{2+}-CaM binding (for CaM not bound to CaMKII) are given in [12] and [14].
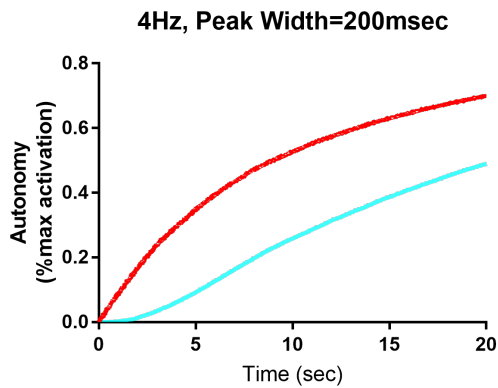
Figure A. Here, we simulate the 2-state-2-step model under identical conditions to those in Figure 3B in De Koninck and Schulman (*Science*, 1998) [15]. Specifically, the model is continuously stimulated by 4Hz Ca^{2+}/CaM with peak widths of 200msec and in the absence of PP. Because the CaMKII subunit concentration is not reported the Schulman study, we use a [CaM] to [CaMKII subunit] ratio of 1:1. We monitor active (red) and pThr-286 (cyan) CaMKII subunits relative to the total concentration of CaMKII subunits (18.24 µM). At t=20sec, our model predicts 50% maximum CaMKII subunit phosphorylation, in agreement with the De Koninck experimental results.

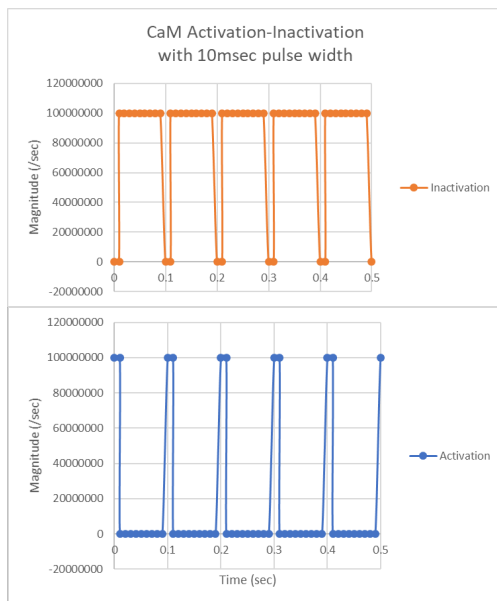Figure B. CaM activation/inactivation parameters as a function of time.

Figure B. Representative traces of the parameters "inactivation" (orange) and "activation" (blue), which in the frequency-dependent simulations vary as a function of time, for the complete duration of the simulation, to force CaM into a fully inactive or active state. Here, we show activation pulse widths at our default value of 10msec.

Text A. Necklace Number Quantification of CaMKII Combinatorial Explosion

In the absence of rules defining the conditions for subunit state transition, CaMKII subunit states are independent, causing combinatorial explosion. To quantify the combinatorial explosion, consider each of the five flags denoting CaMKII subunit states in our model. The docking flag can have one of **two** states. The activation flag can have one of **two** states. The CaM-binding flag can have one of **three** states. The Thr-286 flag can have one of **three** states. Finally, the Thr-306 flag can have one of **two** states. If each flag state is independent, there is a total of **72** possible state combinations that a single subunit can exhibit.

Next, we consider a single ring of six subunits, noting the rotational symmetry. Leveraging this symmetry, we refer to so-called "necklace numbers". Using necklace numbers, the number of fixed arrangements of beads on the necklace is defined as:

$$N(n, a) = \frac{1}{n} \sum_{i=1}^{v(n)} \phi(d_i) \, a^{n/d_i}$$

Where n is the length of the necklace and a is the number of bead types. Phi is Euler's totient function, and d are divisors of n. Thus, for a single CaMKII ring in which n=6 and a=72, the possible number of state combinations is: 23219075544.

To count possible states for a single holoenzyme, we again use necklace numbers. (Squaring the number calculated for a single CaMKII ring fails to account for rare cases in which both rings exhibit identical states.) Thus, we calculate the number of states for the necklace with n=2 and a=23219075544. With this calculation, we determine that in the absence of rules, a twelve-subunit CaMKII holoenzyme as modeled in this paper has **269562734570598985740** possible states.

We emphasize that this value is our estimation. We also acknowledge David Sterratt for his suggestion to use necklace numbers in this calculation.
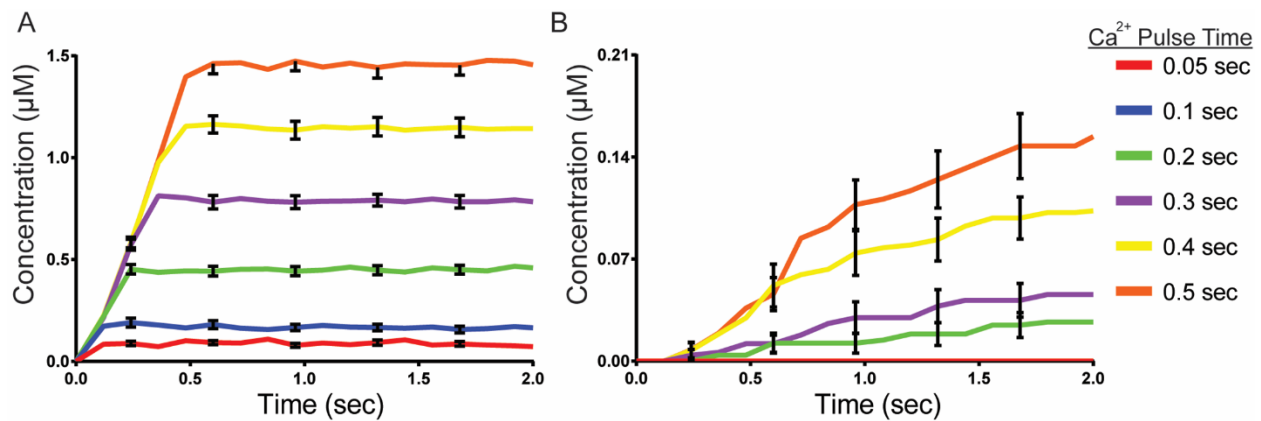
Figure C. Re-creation of Figure 4, showing SEM error bars where all traces are the average of N=50 executions.

Text B. Exploration of Multiple Degrees of Freedom for Autophosphorylation

To explore the dependence of CaMKII pThr-286 patterns on varying mechanisms of autophosphorylation, we present alternative versions of our model in which autophosphorylation may occur in multiple directions, intra- and/or trans-ring. In these higher-degrees of freedom (DoF) models, autophosphorylation may occur in two directions (2 DoF) or three directions (3 DoF).

	1 DoF	2 DoF A	2 DoF B	3 DoF
Intra-ring (Left)	X	X	X	X
Intra-ring (Right)		X		X
Trans-ring (Across)			X	X

Fig D. Schematic of higher-DoF autophosphorylation of CaMKII subunits (blue). Black circles are the enzymes and red circles are the substrate subunits participating in an autophosphorylation.

We hypothesized that higher DoF's could elicit higher or more robust levels of CaMKII autophosphorylation in the presence of phosphatase. Therefore, in Figure E below, we monitor pThr-286 in each of the DoF models as a function of time. Each model is subjected to saturating levels of Ca^{2+}/CaM for 20 sec, after which the stimulating Ca^{2+}/CaM is removed. The results in Figure E indicate that a higher DoF may allow for more rapid formation of pThr-286. For example, the slope of the 3-DoF trace (pink) at t=10sec is noticeably greater than that for the 1-DoF trace (dark blue). Also, following stimulation (after t=20sec) de-phosphorylation rate seems to be independent of DoF. We note that for the models as-simulated and as-parameterized in Figure E, the differences in output between each DoF model may not be experimentally distinguishable.
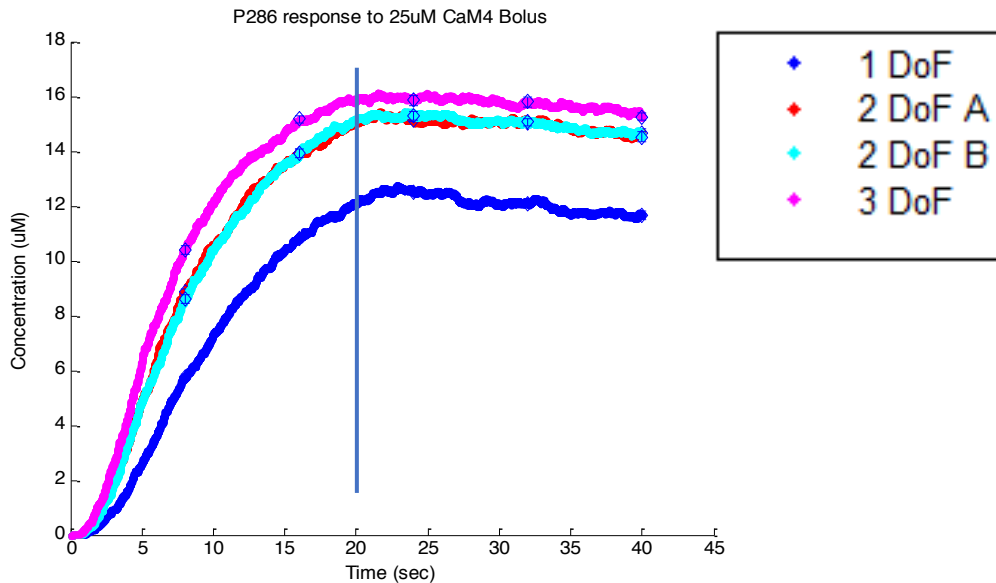
Figure E. Comparing pThr-286 formation for various model DoF for autophosphorylation. For all simulations, holoenzymes were stimulated in the presence of phosphatase with a saturating level of Ca^{2+}/CaM for 20sec, after which Ca^{2+}/CaM was removed. Each trace is the average of N=50 executions.

It is also interesting to consider how a higher DoF could accelerate and/or provide redundant paths by which information (e.g. autophosphorylations) flows from one end of a holoenzyme to the opposite. Indeed, intra-holoenzyme information transfer could impact how CaMKII operates as a simultaneous signaling and structural protein, such as when one subunit interacts with Ca^{2+}/CaM while a neighboring subunit binds to actin [16].

To explore the impact of higher DoF autophosphorylation on intra-holoenzyme information transfer, we use the MCell rule-based modeling syntax to monitor individual subunits on an individual holoenzyme. Monitoring individual subunits allows us to identify CaMKII autophosphorylation "chains", defined as a series of consecutive autophosphorylated subunit neighbors. In Figure F, we monitor individual CaMKII subunit autophosphorylations over time, in the continuous presence of saturating Ca^{2+}/CaM and phosphatase, for various DoFs. In Figure G, we quantify the dependence of autophosphorylation chain formation on DoF number. Increasing DoF increases the lifetime of autophosphorylation chains (of any length), albeit marginally leading us to suspect experimental measurements would be inconclusive.
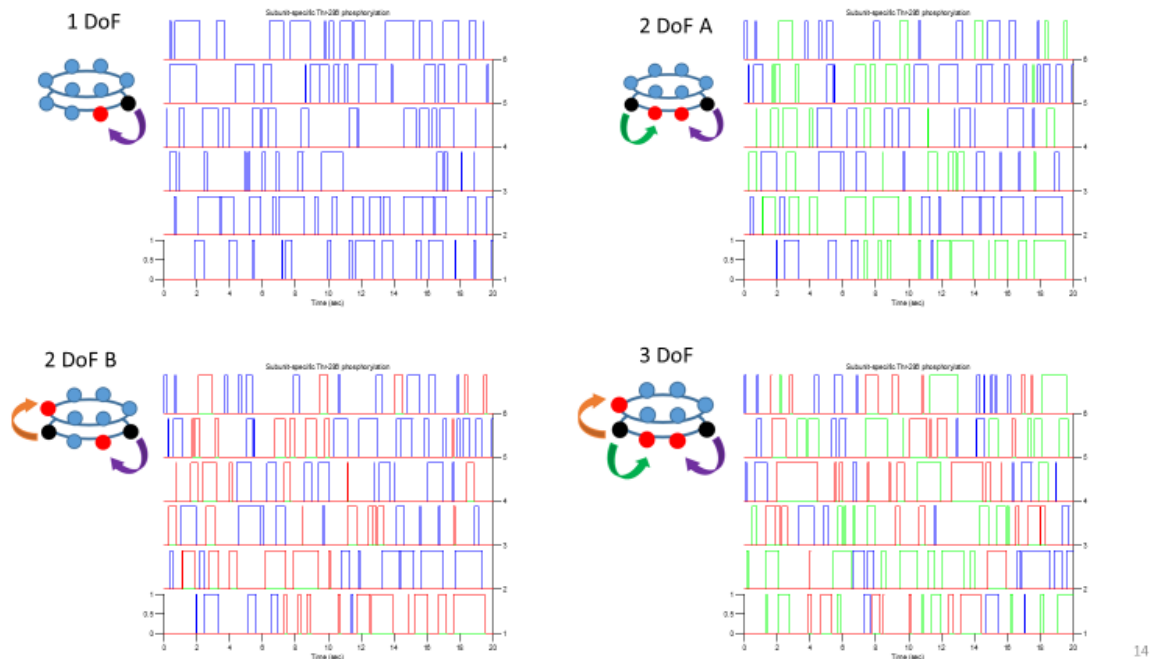
Figure F. Monitoring individual CaMKII subunits at distinct autophosphorylation DoF. In each panel, the horizonal axis is time (up to 20 sec). Each row pertains to one of six subunits in a single holoenzyme ring, and each trace is a binary representation of whether that subunit is pThr-286 (one) or uThr-286 (zero). Depending on the number of DoF, autophosphorylations may proceed clockwise (blue), counter-clockwise (green), and/or trans-ring (red).
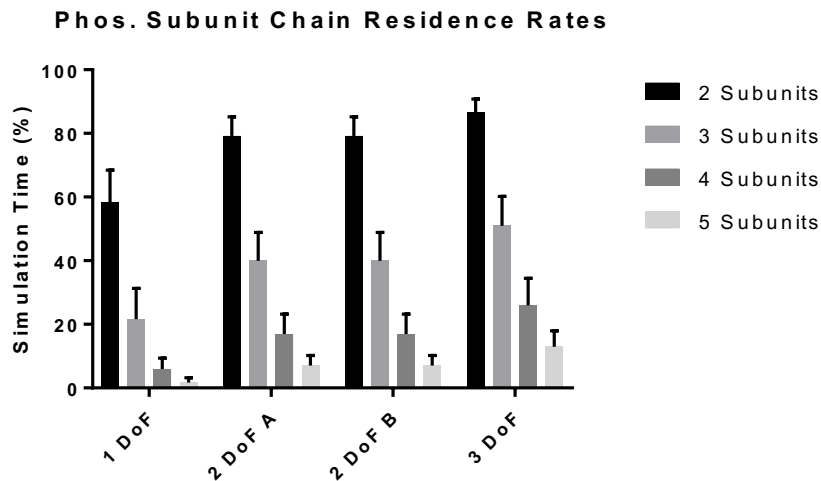

Figure G. pThr-286 chain occurrence increases with increasing DoF. Here, we monitored a single CaMKII holoenzyme over 2min. Each bar denotes the fraction of time that a chain of length n occurs for that number of DoF. Each bar is the average of N=50 executions.

Movie A.

Please see this link - https://youtu.be/lUSuv2mWa5g.

Text C. Discussion of putative PP1-CaMKII binding site.

Many PP1-binding proteins contain a variable binding motif commonly called the RVxF binding motif [17]. However, no such motif is seen in the alpha-CaMKII subunit amino acid sequence. Furthermore, no structure for the PP1-CaMKII interaction exists, in part because apo-PP1 is unstable in solution [18]. We can instead refer to a crystal structure published by Ragusa *et al*., which shows PP1 binding the neuronal regulatory protein spinophilin (PDB 3EGG) [19].

The 3EGG crystal structure shows an interaction with PP1 spanning the spinophilin residues 417-494. This interaction involves 77 residues (~100 Å, see Figure H), which are necessary and sufficient for PP1 to dephosphorylate spinophilin [20]. This interaction distance is longer than the CaMKII regulatory domain and CaM-binding footprint. Indeed, the CaMKII regulatory domain is only about 39 Å (as in PDB 3SOA, partially shown in Figure I).
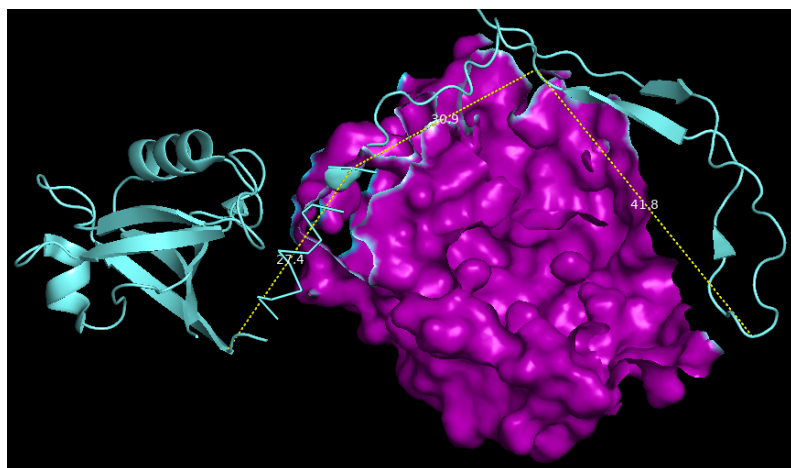

Figure H. Visualization of the spinophilin (cyan) and PP1 (purple) binding interaction (PDB: 3EGG). Some of the PP1 surface is digitally removed to help visualize the dotted lines, which together approximate the distance spanned by spinophilin residues 417-494.
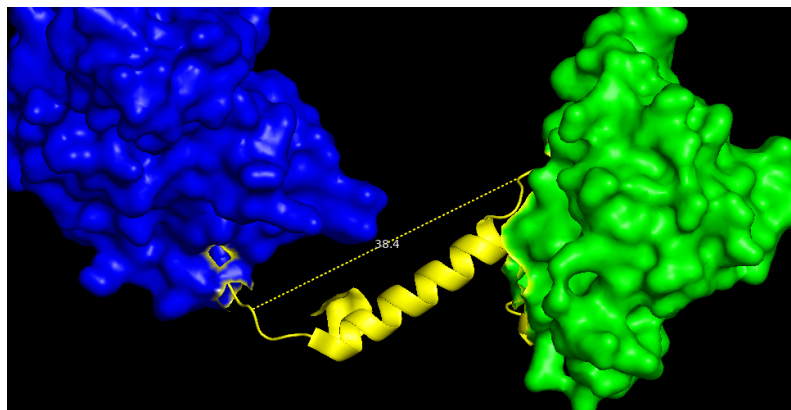

Figure I. Visualization of the CaMKII regulatory domain (yellow) (PDB: 3SOA). The CaMKII hub domain (green) and kinase domain (blue) are also shown. Dotted line measures from residues 280-306.

Note also that the typical PP1 binding motif interacts with PP1 at a site roughly 20 Å from the PP1 active site [20]. Thus, if the PP1 binding footprint does not contain T286, then the furthest CaMKII residue the PP1 footprint could likely be (on the hub domain side of T286) is residue 301, well within the CaM-

binding footprint (see Figure J). Admittedly, the furthest likely PP1-binding residue on the kinase domain side of T286 is difficult to ascertain from PDB 3SOA. Still, we believe there is strong evidence that CaM structurally excludes or limits PP1 from binding and/or catalyzing de-phosphorylation at T286.
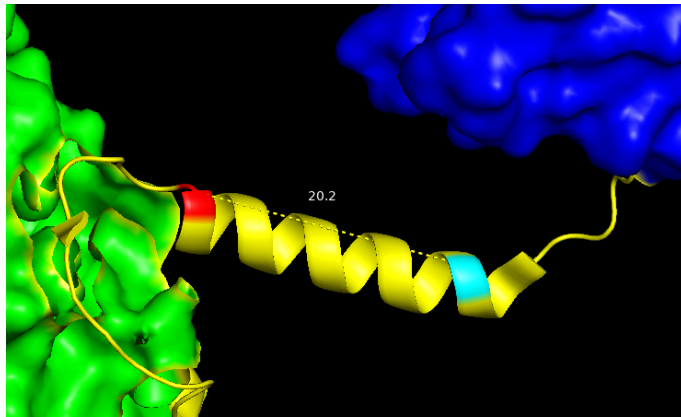

Figure J. Visualization of the furthest likely residue (G301; red) of PP1-binding on the hub domain (green) side of T286 (cyan) (PDB: 3SOA). Dotted line measures from residues 286-301.

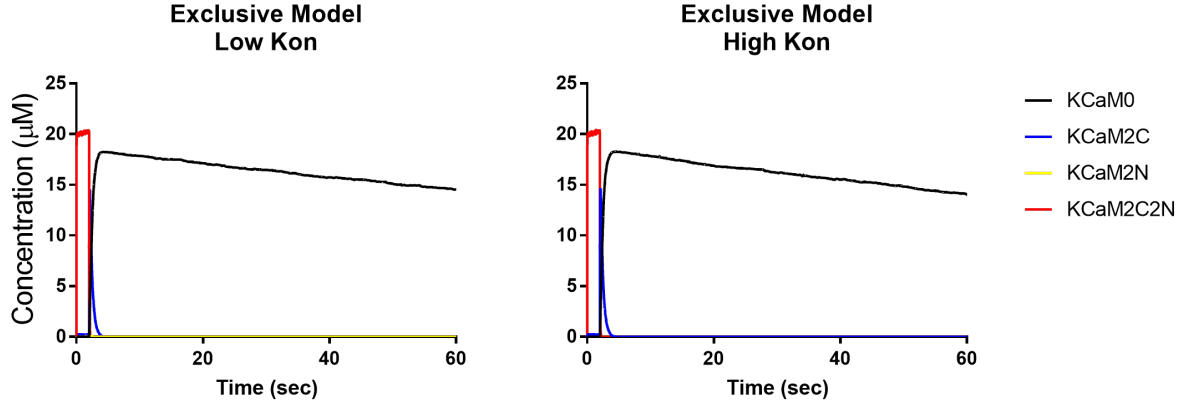## Figure K. Major Ca^{2+}/CaM-CaMKII states following Ca^{2+} bolus in the 9-state-1-step model

Figure K. Bound Ca^{2+}/CaM states in response to 2 sec Ca^{2+} bolus as-implemented in Fig 7. We monitor the CaMKII-bound Ca^{2+}/CaM states apo-CaM (black), CaM$_{2C}$ (blue), CaM$_{2N}$ (yellow), and CaM$_4$ (or CaM$_{2C2N}$, red) in the PP1-exclusive 9-state-1-step model under low (left) and high (right) association rate parameters for PP1-CaMKII binding. Each trace is the average of N=20 executions.

Figure L. Ca^{2+}/CaM-CaMKII states with dynamic Ca^{2+} stimulation and the 9-state-1-step model
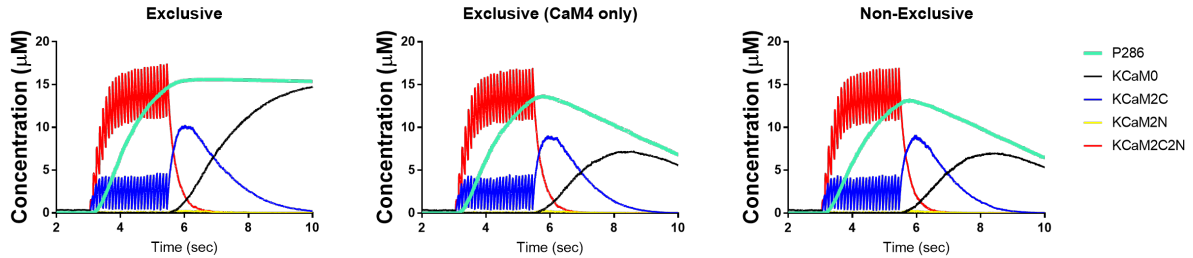

Figure L. CaMKII-bound Ca^{2+}/CaM states and pThr-286 subunits (cyan) in response to 10Hz Ca^{2+} flux. Peak pThr-286 levels at t=6 sec are highest in the exclusive model (15.4 μM). When only CaM$_4$ is allowed to exclude PP1-binding, pThr-286 levels at t=6 sec are 13.5 μM, whereas pThr-286 levels at the same time point in the non-exclusive model are 13 μM. Also, at t=10 sec pThr-286 levels in the non-exclusive model are lower (6.4μM) than when only CaM$_4$ excludes PP1-binding (7μM), seemingly due to heightened CaM$_{2C}$ levels immediately following termination of Ca^{2+} flux. Altogether, it seems that during and immediately following dynamic Ca^{2+} flux, CaM$_{2C}$ levels may be non-negligible. CaM$_{2C}$, in addition to apo-CaM or CaM$_4$, could sometimes significantly regulate pThr-286 levels via CaM-dependent PP1 exclusion. Because this is the 9-state-1-step model, each trace is the average of N=20 executions.

References (Supplement)

1.	Torok K, Tzortzopoulos A, Grabarek Z, Best SL, Thorogate R. Dual effect of ATP in the activation mechanism of brain Ca2+/calmodulin-dependent protein kinase II by Ca2+/calmodulin. Biochemistry. 2001;40(49):14878-90. doi: 10.1021/bi010920+.
2.	Tzortzopoulos A, Torok K. Mechanism of the T286A-mutant alpha CaMKII interactions with Ca2+/calmodulin and ATP. Biochemistry. 2004;43(21):6404-14. doi: 10.1021/bi036224m.
3.	Chao LH, Stratton MM, Lee IH, Rosenberg OS, Levitz J, Mandell DJ, et al. A Mechanism for Tunable Autoinhibition in the Structure of a Human Ca2+/Calmodulin-Dependent Kinase II Holoenzyme. Cell. 2011;146(5):732-45. doi: 10.1016/j.cell.2011.07.038.
4.	Stefan MI, Marshall DP, Le Novere N. Structural analysis and stochastic modelling suggest a mechanism for calmodulin trapping by CaMKII. PLoS One. 2012;7(1):14. doi: 10.1371/journal.pone.0029406.
5.	Hoffman L, Chandrasekar A, Wang X, Putkey JA, Waxham MN. Neurogranin alters the structure and calcium binding properties of calmodulin. J Biol Chem. 2014;289(21):14644-55. doi: 10.1074/jbc.M114.560656.
6.	Hoffman L, Stein RA, Colbran RJ, McHaourab HS. Conformational changes underlying calcium/calmodulin-dependent protein kinase II activation. Embo J. 2011;30(7):1251-62. doi: 10.1038/emboj.2011.40.
7.	Tse JKY, Giannetti AM, Bradshaw JM. Thermodynamics of calmodulin trapping by Ca2+/calmodulin-dependent protein kinase II: Subpicomolar K-d determined using competition titration calorimetry. Biochemistry. 2007;46(13):4017-27. doi: 10.1021/bi700013y.
8.	Shifman JM, Choi MH, Mihalas S, Mayo SL, Kennedy MB. Ca2+/calmodulin-dependent protein kinase II (CaMKII) is activated by calmodulin with two bound calciums. Proc Natl Acad Sci U S A. 2006;103(38):13968-73. doi: 10.1073/pnas.0606433103.
9.	Zhabotinsky AM. Bistability in the Ca2+/calmodulin-dependent protein kinase-phosphatase system. Biophys J. 2000;79(5):2211-21. doi: 10.1016/s0006-3495(00)76469-1.
10.	Lucic V, Greif GJ, Kennedy MB. Detailed state model of CaMKII activation and autophosphorylation. Eur Biophys J Biophys Lett. 2008;38(1):83-98. doi: 10.1007/s00249-008-0362-4.
11.	Payne ME, Fong YL, Ono T, Colbran RJ, Kemp BE, Soderling TR, et al. Calcium calmodulin-dependent protein kinase-II - characterization of distinct calmodulin binding and inhibitory domains. J Biol Chem. 1988;263(15):7190-5.
12.	Pepke S, Kinzer-Ursem T, Mihalas S, Kennedy MB. A dynamic model of interactions of Ca2+, calmodulin, and catalytic subunits of Ca2+/calmodulin-dependent protein kinase II. PLoS Comput Biol. 2010;6(2):15. doi: 10.1371/journal.pcbi.1000675.
13.	Meyer T, Hanson PI, Stryer L, Schulman H. Calmodulin trapping by calcium-calmodulin dependent protein-kinase. Science. 1992;256(5060):1199-202. doi: 10.1126/science.256.5060.1199.
14.	Romano DR, Pharris MC, Patel NM, Kinzer-Ursem TL. Competitive tuning: Competition's role in setting the frequency-dependence of Ca2+-dependent proteins. PLoS Comput Biol. 2017;13(11):26. doi: 10.1371/journal.pcbi.1005820.
15.	De Koninck P, Schulman H. Sensitivity of CaM kinase II to the frequency of Ca2+ oscillations. Science. 1998;279(5348):227-30. doi: 10.1126/science.279.5348.227.
16.	Lisman JE, Zhabotinsky AM. A model of synaptic memory: A CaMKII/PP1 switch that potentiates transmission by organizing an AMPA receptor anchoring assembly. Neuron. 2001;31(2):191-201. doi: 10.1016/s0896-6273(01)00364-6.
17.	Cohen PTW. Protein phosphatase 1 - targeted in many directions. J Cell Sci. 2002;115(2):241-56. PubMed PMID: WOS:000173768800002.
18.	Kelker MS, Page R, Peti W. Crystal structures of protein phosphatase-1 bound to nodularin-r and tautomycin: a novel scaffold for structure-based drug design of serine/threonine phosphatase inhibitors. J Mol Biol. 2009;385(1):11-21. doi: 10.1016/j.jmb.2008.10.053.

19.	Ragusa MJ, Dancheck B, Critton DA, Nairn AC, Page R, Peti W. Spinophilin directs protein phosphatase 1 specificity by blocking substrate binding sites. Nat Struct Mol Biol. 2010;17(4):459-U100. doi: 10.1038/nsmb.1786.
20.	Hsieh-Wilson LC, Allen PB, Watanabe T, Nairn AC, Greengard P. Characterization of the neuronal targeting protein spinophilin and its interactions with protein phosphatase-1. Biochemistry. 1999;38(14):4365-73. doi: 10.1021/bi982900m.